

Phase diagram of highly asymmetric binary hard-sphere mixtures

Marjolein Dijkstra, René van Roij, and Robert Evans

H. H. Wills Physics Laboratory, University of Bristol, Royal Fort, Bristol BS8 1TL, United Kingdom

(Received 23 December 1998)

We study the phase behavior and structure of highly asymmetric binary hard-sphere mixtures. By first integrating out the degrees of freedom of the small spheres in the partition function we derive a formal expression for the effective Hamiltonian of the large spheres. Then using an explicit pairwise (depletion) potential approximation to this effective Hamiltonian in computer simulations, we determine fluid-solid coexistence for size ratios $q=0.033, 0.05, 0.1, 0.2,$ and 1.0 . The resulting two-phase region becomes very broad in packing fractions of the large spheres as q becomes very small. We find a stable, isostructural solid-solid transition for $q \leq 0.05$ and a fluid-fluid transition for $q \leq 0.10$. However, the latter remains metastable with respect to the fluid-solid transition for all size ratios we investigate. In the limit $q \rightarrow 0$ the phase diagram mimics that of the sticky-sphere system. As expected, the radial distribution function $g(r)$ and the structure factor $S(k)$ of the effective one-component system show no sharp signature of the onset of the freezing transition and we find that at most points on the fluid-solid boundary the value of $S(k)$ at its first peak is much lower than the value given by the Hansen-Verlet freezing criterion. Direct simulations of the true binary mixture of hard spheres were performed for $q \geq 0.05$ in order to test the predictions from the effective Hamiltonian. For those packing fractions of the small spheres where direct simulations are possible, we find remarkably good agreement between the phase boundaries calculated from the two approaches—even up to the symmetric limit $q=1$ and for very high packings of the large spheres, where the solid-solid transition occurs. In both limits one might expect that an approximation which neglects higher-body terms should fail, but our results support the notion that the main features of the phase equilibria of asymmetric binary hard-sphere mixtures are accounted for by the effective pairwise depletion potential description. We also compare our results with those of other theoretical treatments and experiments on colloidal hard-sphere mixtures. [S1063-651X(99)07805-8]

PACS number(s): 82.70.Dd, 61.20.Gy, 64.70.-p

I. INTRODUCTION

The theory of the structure and phase behavior of simple (atomic) fluids relies heavily on our knowledge of the hard-sphere system, which serves as a standard reference system for determining the properties of more realistic models. As such the hard-sphere system has been studied in great detail during the past few decades and its phase behavior is now well understood. In particular, it was shown by computer simulations that a system of identical hard spheres has a well-defined freezing transition [1,2] driven by purely entropic effects. Pure hard spheres do not undergo a liquid-gas transition since this requires a source of attractive interactions. The state of affairs for the binary hard-sphere mixture is less clear-cut and the phase behavior is still hotly debated. This system plays a similar (reference) role for binary mixtures of simple fluids and also serves as a model for mixtures of colloids and polymers, or other colloidal systems. The main issue is whether a binary fluid mixture of large and small hard spheres is miscible for all size ratios and compositions or whether a fluid-fluid demixing transition takes place and, if it does, whether such a transition is stable or metastable with respect to the fluid-solid transition. The discussion was instigated in 1991 by Biben and Hansen, who showed within an integral equation theory that the binary hard-sphere mixture exhibits a spinodal instability in a high-density fluid when the size ratio of the two species is more extreme than 1:5 [3]. As this result was in contradiction with a classic study by Lebowitz and Rowlinson, who had concluded that the mixture is stable against demixing regardless

of the state point and the size ratio [4], it initiated renewed interest in this system. Despite all the work that has since been devoted to this issue, it remains an unresolved question as to whether a stable fluid-fluid demixing transition exists in hard-sphere mixtures. The physical mechanism behind (possible) demixing in hard-sphere mixtures is the depletion effect. This is based on the idea that clustering of the large spheres allows more free volume for the small ones which may lead to an increase in the entropy, i.e., to a lowering of the free energy. The depletion effect is known to lead to demixing in colloid-polymer mixtures but it is not known whether this is sufficiently strong to bring about demixing in *additive* mixtures of hard spheres. In such mixtures the pairwise potential between species 1 and 2 is described by a diameter σ_{12} which is the mean of those for like-like interactions: $\sigma_{12} = (\sigma_{11} + \sigma_{22})/2$. Colloid-polymer mixtures are usually treated by a model which assumes the polymer-polymer interactions to be ideal so that the hard-sphere diameters are nonadditive. Here we focus on additive binary hard-sphere mixtures, thereby ignoring recent work on binary hard-core mixtures of nonspherical particles [5,6] and polydispersity [7], and we mention briefly results for nonadditive mixtures where these are relevant.

One might suppose that computer simulations should have resolved the issues concerning the phase behavior. However, direct simulations of highly asymmetric binary mixtures are prohibited by slow equilibration when the packing fraction of the small spheres becomes substantial and there have been no systematic attempts to calculate phase diagrams for the asymmetric cases which are of most inter-

est. On the theoretical side it is now well accepted that those approaches which attempt to treat both species on an equal footing, e.g., integral equation theories or virial expansions of the mixture equation of state, yield results which are notoriously sensitive to the details of the approximations. The (non)existence and location of the spinodal instability is particularly susceptible but the location of the fluid-solid phase boundary is also very sensitive to the choice of approximation. In the present paper we adopt a different strategy which takes advantage of the large-size asymmetry: we integrate out the degrees of freedom of the small spheres and obtain an effective Hamiltonian for the larger ones. The effective Hamiltonian consists of zero-body, one-body, two-body, and higher-body interactions which depend on the density of the small spheres. We employ a simplified version, which consists of only pairwise additive depletion potentials between the larger spheres, in Monte Carlo simulations. We find a fluid-fluid demixing transition for size ratios of 1:10 or more extreme. However, this transition is metastable with respect to the fluid-solid transition which occurs at strikingly small values of the packing fraction of the large spheres. More surprisingly, perhaps, we also find an isostructural solid-solid transition at high packing fractions of the large spheres. This transition becomes stable for a size ratio ≤ 0.05 . The richness of the predictions from the approximate effective Hamiltonian leads us to attempt direct simulations of the true binary hard-sphere mixture. These *are* feasible for size ratios ≥ 0.05 , provided the density of the small spheres is fairly low. We find remarkably good agreement between the results of the two sets of simulations even in the solid phase(s) and for relatively large size ratios (0.2) where one might expect the approximation of pairwise additivity to fail. The success of our comparison implies that an effective Hamiltonian approach based on a pairwise depletion potential description should provide an accurate, albeit approximate, account of the main features of the phase behavior of highly asymmetric hard-sphere mixtures.

The paper is organized as follows: In Sec. II we give an historical overview of research on additive binary hard-sphere mixtures. This is not intended as a comprehensive review; rather, it should provide a more detailed introduction to earlier work and motivation for our present approach. In Sec. III the effective Hamiltonian is derived by integrating out the degrees of freedom of one of the species in a binary mixture. We emphasize that this derivation is not restricted to a binary hard-sphere mixture; it applies to any two-component mixture where the species interact via short-ranged pairwise potentials. The theory is applied to additive binary hard-sphere mixtures in Sec. IV where explicit formulas are introduced for the one-body and two-body (depletion potential) contributions. Results of computer simulations based on the approximate effective Hamiltonian are presented in Sec. V. The phase diagrams and the pairwise correlation functions are calculated for a range of size ratios. In Sec. VI we present the results of the direct simulations of the true binary mixture and compare the phase diagrams with those obtained from the effective Hamiltonian. Section VII A makes comparisons between our present results and those of experiment and previous theories or simulations, while in Sec. VII B we make a connection with the so-called free volume theory of binary hard-sphere mixtures, showing how

that approach relates to the present. Finally, in Sec. VII C we make some concluding remarks. Some of our results have been presented in short communications [8,9].

II. HISTORICAL OVERVIEW

In the early days of liquid state physics it was not clear whether attraction was necessary to drive a freezing transition in simple fluids. In 1957 Wood and Jacobson [1] and Alder and Wainwright [2] showed by computer simulations that a system of purely repulsive hard spheres has a well-defined freezing transition. These results were disputed for a long period, but nowadays it is generally accepted that a system of identical hard spheres does have a fluid-solid transition [10]. The origin of this freezing transition is purely entropic and occurs because the entropy of the crystalline phase is higher than that of the fluid phase at sufficiently high densities.

In a simple picture of a solid all molecules are confined to cells centered at lattice sites. This confinement results in a decrease in entropy. At sufficiently high density, however, the molecules in a dense fluid will be more jammed than in a solid, where the molecules can move freely within cells. This increase in free volume per molecule in a solid results in a gain in entropy that can outweigh the loss in entropy incurred by confining the molecules to cells.

The location of this hard-sphere freezing transition was determined from simulations by Hoover and Ree, who found that the packing fractions of the coexisting fluid and face-centered cubic solid phase (fcc) are given by $\eta^{\text{fluid}}=0.494$ and $\eta^{\text{solid}}=0.545$, which corresponds to a pressure $P\sigma^3/k_B T=11.69$ with σ the diameter of the hard spheres [11]. We also note that it has been shown recently that at coexistence the fcc crystal is indeed more stable than the hexagonal close-packed (hcp) crystal [12].

In the last decade, it was found that binary hard-sphere mixtures show extremely rich phase behavior. A density functional treatment of Barrat, Baus, and Hansen showed that starting from the pure limit, the freezing transition of the mixture changes from a spindlelike transition via an azeotropic to an eutecticlike one when the two species become more dissimilar in size [13]. In the case of spindlelike phase behavior, a narrow coexistence is found between a fluid and a substitutionally disordered fcc crystal. Here ‘‘narrow’’ refers to the width of this coexistence region expressed in terms of the composition difference between the two coexisting phases. When the spheres become more dissimilar in size, the fluid-solid region broadens and an azeotropic point appears. At higher packing fractions a coexistence region between two substitutionally disordered fcc solids appears in the phase diagram when the spheres become sufficiently dissimilar. When this miscibility gap in the solid phase intervenes with the fluid-solid coexistence the phase diagram becomes eutecticlike. Computer simulations, other density functional approaches, and a scaled particle approach revealed that these predictions are qualitatively correct [14–19]: the transition from a spindle to azeotropic type of phase diagram is predicted at a size ratio $q=\sigma_2/\sigma_1=0.94$ [13,14] and the transition from azeotropic to eutectic at $q=0.92$ [13] or 0.875 [14]. The diameters of the large and small spheres are, respectively, σ_1 and σ_2 . Note that only substitutionally

disordered fcc solids are found for these size ratios.

In recent experiments, however, complex crystalline order is found for $q=0.58$ and 0.62 [20]. For sterically stabilized polymethylmetacrylate (PMMA) spheres, AB_2 and AB_{13} superlattice structures are found, where A denotes the larger species. The presence of these superlattice structures as stable phases was subsequently confirmed by computer simulations for $0.41 \leq q \leq 0.625$ [21] and by density functional approaches [22]. In addition, it was shown that the fluid phase never undergoes fluid-fluid demixing for these size ratios. Thus the phase behavior of binary hard-sphere mixtures is well understood for $q > 0.4$.

This state of affairs should be contrasted with the case of more asymmetric binary hard-sphere mixtures, the phase behavior of which is still under debate. For instance, it is still unclear whether a (stable) fluid-fluid demixing transition can exist for any binary hard-sphere mixture. In 1964, Lebowitz and Rowlinson showed, using the Percus-Yevick (PY) closure of the Ornstein-Zernike (OZ) equations, that the homogeneous fluid phase of a binary mixture of large and small hard spheres is stable with respect to demixing, regardless of the diameter ratio, composition, or pressure [4]. A similar prediction emerged from the generalization of Mansoori *et al.* of the Carnahan-Starling equation of state for mixtures; i.e., no spinodal instability was found in the fluid phase [23]. Computer simulations of binary hard-sphere mixtures for $q = 0.6$ [24], 0.909 [25], 0.5 and 0.33 [26], 0.33 [27], 0.909 , 0.6 , 0.33 , 0.2 , and 0.05 [28], performed for packings where ergodicity problems do not prevent equilibration, did not provide any evidence for a demixing transition, and it was therefore generally believed that binary hard-sphere mixtures never phase separate into two fluid phases. In 1990, however, Biben and Hansen showed that the pair distribution function diverges at contact, within the Percus-Yevick approximation, in the extreme asymmetric limit $q \rightarrow 0$ [29]. One year later, the same authors showed that the Rogers-Young (RY) closure, which for the pure hard-sphere system is known to be more accurate than the Percus-Yevick closure, yields a fluid spinodal instability when $q \leq 0.2$ [3]. They attributed the fluid spinodal to the stickiness of the large particles arising from the so-called *depletion effect*. This effect, which has long been known to drive phase separation in colloid-polymer mixtures [30,31], induces effective attractions between large (colloidal) spheres at small separations due to an unbalanced pressure of small (polymeric) spheres. An alternative description of the same effect is that a free volume of the small spheres is gained due to the overlap of the excluded volume of clustering large spheres; the resulting gain of entropy of the small spheres drives this clustering, and thus induces effective attractions between the large spheres. In 1993, this latter picture of the depletion effect was employed by Lekkerkerker and Stroobants in a phenomenological approach based on scaled particle expressions for the free volume [32]. In qualitative agreement with the results of Ref. [3], these authors found a fluid-fluid spinodal [32]. However, the spinodal instability in Ref. [32] shifts to higher packing fractions of the small spheres when the size ratio becomes more asymmetric, while the opposite trend is to be expected since the depletion effect becomes stronger for more asymmetric hard-sphere mixtures. Moreover, it was shown by Amokrane and Regnaut that the location of the

spinodal instability is very sensitive to the precise expression used for the free volume [33]. In 1995 Rosenfeld employed his fundamental-measures density functional theory to asymmetric binary hard-sphere systems, and predicted a fluid-fluid demixing transition for a size ratio $q \leq 0.25$ [34].

These early theories for asymmetric binary hard-sphere mixtures did not consider the crystalline solid phase explicitly. However, experiments on colloidal (nearly) hard-sphere particles suggest that any demixing transition is strongly coupled to the freezing transition. Unfortunately, surface crystallization and sedimentation effects preclude making definite conclusions. For instance, Sanyal *et al.* performed experiments on mixtures of polystyrene spheres with a diameter ratio of 0.2 [35], and observed cluster formation in the sediment at the bottom of their samples. In contrast, when they suspended the mixture in a density-matched solvent, neither sedimentation nor flocculation was seen. In the experiments of van Duijneveldt *et al.*, a phase instability was found in a fairly narrow concentration range of small and large silica particles with $q = 0.1667$ [36]. However, in these experiments conclusions could only be drawn during the first few hours, as sedimentation becomes important at longer times. Thus the authors could not determine whether the phases formed initially in the samples outside this narrow concentration range were stable fluid phases or metastable fluids or glasses. They also concluded that the crystallization, observed in the sediment after several weeks, could be caused either by slow concentration-dependent kinetics or by densification to the freezing point arising from sedimentation. Experiments on mixtures of polystyrene particles with size ratios $0.069 \leq q \leq 0.294$ by Kaplan *et al.* showed the existence of either a single homogeneous disordered phase, a coexistence between two disordered phases, a coexistence between a disordered phase and a crystal on the sample wall, or coexistence between two disordered bulk phases and a surface crystallization [37]. However, bulk crystallization was never observed. A possible reason why no surface crystallization was found in the experiments of van Duijneveldt *et al.* is the fast settling of silica spheres compared to polystyrene particles. Dinsmore *et al.* reported results on mixtures of polystyrene particles with $0.083 \leq q \leq 0.149$ [38]. In addition to surface crystallization, they observed fluid-solid phase separation at higher packing fractions of small spheres. When they increased the packing fraction of the small spheres even further, they observed that the clusters in the sediment rapidly form a ‘‘loose’’ gel instead of a crystal. Independently, Imhof and Dhont found a fluid-solid type of phase separation in experiments on silica spheres with $q = 0.1075$ [39]. Moreover, two types of glassy states, distinguished by the different mobilities of the small spheres, were found at high packing fractions of the large spheres. In both cases the large ones form a glasslike structure whereas the small ones are mobile (fluidlike) in one case and rather immobile in the other.

Inspired by these experimental results, Poon and Warren [40] and Dinsmore *et al.* [41] extended the free volume approach of Lekkerkerker and Stroobants [32] to the solid phase and concluded that the fluid-fluid demixing transition should be metastable with respect to a broad fluid-solid coexistence region. In addition they found that the presence of small spheres causes crystallization of large spheres next to a

hard wall at concentrations well below those corresponding to bulk phase separation, in agreement with the experimental observations. A broad fluid-solid coexistence has also been found in density functional calculations based on the modified weighted density approximation for a binary hard-sphere mixture with $q=0.1$ [42]. Recently Caccamo and Pellicane showed, using a single-phase entropic freezing criterion and the thermodynamically self-consistent Rogers-Young theory, that for a single state point the phase instability in binary hard-sphere mixtures with $q=0.1$ is consistent with fluid-solid phase separation [43]. Another freezing criterion was employed by Saija and Giaquinta [44]. A different approach, based on results for the first five virial coefficients of the binary hard-sphere mixture, was adopted by Coussaert and Baus [45,46]. In addition to a fluid-solid transition they find a thermodynamically stable fluid-fluid transition for size ratios as large as $q=0.15$ and $q=0.33$ [45], if the fourth and fifth virial coefficients are taken from results of Saija *et al.* [47]. However, in a subsequent erratum which uses the fourth and fifth virial coefficients from Enciso *et al.* [48], they find that the fluid-fluid transition is at such high packing fractions that they argue it should be metastable with respect to a broad fluid-solid transition for $q=0.2$ and a narrow one for $q=0.1$ [46]. Yet another theoretical treatment by Vega predicts a narrow fluid-solid coexistence for $q \rightarrow 0$ [49]. In summary the predicted phase behavior of asymmetric binary hard-sphere mixtures is very sensitive to the details of the theoretical approaches, and the character of the fluid-fluid and fluid-solid transitions and their interplay remains poorly understood.

In this paper we explore an alternative route to the phase behavior of asymmetric binary hard-sphere mixtures. It is based on our present knowledge of the depletion force between two big spheres immersed in a fluid of small particles. When the separation of the big spheres is less than the diameter of the small ones, there is an unbalanced pressure of the “sea” of small spheres which gives rise to the attractive depletion force between the big spheres. As mentioned above this mechanism was first described by Asakura and Oosawa for colloid-polymer mixtures [30]. The depletion force was investigated in detail by Attard and co-workers within hypernetted-chain-based approximations [50] and in simulations [51]. Mao *et al.* calculated the depletion force up to third order in the density of the smaller spheres [52], having first made the Derjaguin approximation to relate the force between the two big spheres to that which arises when the small particles are confined between two planar walls. They found good agreement with the simulation results for $q=0.1$ of Biben *et al.* [53]. Götzelmann *et al.* [54] have recently assessed various theoretical treatments of the depletion force and the corresponding depletion potential $\phi_{\text{dep}}(r)$. Depletion potentials have also been “measured” experimentally. Kaplan *et al.* performed experiments for a large sphere near a wall in a suspension of small spheres. By tracking the Brownian trajectory of the large sphere with video microscopy, they were able to determine the potential depth, which they estimated to be of the order of a few $k_B T$ for a size ratio of 0.028 [55]. Ye *et al.* measured the structure factor of the big colloidal particles in a neutron scattering experiment on colloid-polymer mixtures. By fitting these structure factors to those calculated from the Asakura-Oosawa depletion pair po-

tential (using the random phase approximation), they found that the depth of the depletion potential increases linearly with (low) polymer concentration, as predicted by the Asakura-Oosawa approximation [56]. Laser radiation experiments were used to measure the minimum laser intensity that is required to blow off a large polystyrene latex particle from the wall as a function of polymer concentration [57]. These laser intensities were translated into depletion forces and again good agreement was found with the Asakura-Oosawa depletion force. Depletion forces of colloidal hard spheres trapped in a vesicle were measured by Dinsmore *et al.* [58]. They found that the large particles are more likely to be trapped close to regions of the surface which have a large curvature and they argue the importance of their results for biological systems [58]. Very recently, Rudhardt *et al.* [59] measured the depletion force on a large polystyrene sphere immersed in a solution of small, noncharged polymers as a function of the *distance* to a flat glass surface and of *polymer concentration* using total internal reflection microscopy. They also find good agreement with theoretical predictions [59]. Finally, we mention that the depletion potential was measured recently using optical tweezers [60] and good agreement with the Asakura-Oosawa depletion potential was claimed.

Of course, one should bear in mind that real colloidal mixtures or colloid-polymer mixtures are not strictly binary hard-sphere mixtures, and so there are possible influences from screened Coulomb forces, polydispersity, etc., which make direct comparison between experiment and theory based on idealized models a matter for some caution.

In view of all the theoretical and experimental effort which has been expended on determining depletion potentials it is somewhat surprising, perhaps, that these potentials have not been used to calculate the phase behavior of binary hard-sphere mixtures. One might envisage performing simulations or carrying out theoretical studies for an effective one-component system in which the big spheres interact via a pairwise potential $\phi_{\text{eff}} = \phi_{11} + \phi_{\text{dep}}$, where ϕ_{11} is the hard-sphere potential between the two big spheres and ϕ_{dep} is the depletion potential obtained from the theoretical or simulation treatments described above. Recall that ϕ_{dep} depends on the density of the small spheres. Such a strategy was employed by Gast *et al.* [61] in a pioneering investigation of the phase behavior of colloid-polymer mixtures. However, a systematic derivation of an effective Hamiltonian, obtained by integrating out the degrees of freedom of the small spheres, was not carried out, and so the status of the effective pairwise depletion potential description has remained uncertain. Moreover, Ref. [61] specializes to the case of ideal polymers, for which the Asakura-Oosawa potential is appropriate, rather than the case of additive binary hard-sphere mixtures. (We make contact with the results of Ref. [61] in later sections.) In the present work we derive an effective Hamiltonian by formally integrating out the degrees of freedom of the small spheres. We show that this Hamiltonian has zero-body, one-body, two-body, and higher-body terms. The two-body (pairwise) term is precisely that which is given by the depletion potential description and we show that the zero-body and one-body terms play no role in determining phase equilibria. Ignoring the higher-body terms we perform simulations with the effective pairwise potential defined above

and ϕ_{dep} obtained from Ref. [54]. We thus determine the phase behavior of binary hard-sphere mixtures for size ratios $q = 1.0, 0.2, 0.1, 0.05,$ and 0.033 . As the results of these effective one-component calculations predict several striking features at relatively low values of the density of small spheres we were motivated to perform direct simulations of the binary hard-sphere system in order to test these predictions. The results from the two sets of simulations are in remarkably good agreement for those values of q and packing fractions for which direct simulations are possible, thereby justifying the use of the effective pairwise depletion description.

III. GENERAL THEORY OF BINARY MIXTURES

A. Mapping onto an effective one-component system

Here we formally map a system with interaction Hamiltonian H that describes a binary mixture onto an effective one-component system with Hamiltonian H^{eff} by integrating out the degrees of freedom of one species. We are concerned with a classical fluid of two species, labeled 1 and 2, in a macroscopic volume V . For particle numbers N_1 and N_2 , the total Hamiltonian $\mathcal{H} = K + H$ is a sum of kinetic energy K and interaction energy $H = H_{11} + H_{12} + H_{22}$, given by

$$\begin{aligned} K &= \sum_{i=1}^{N_1} \frac{\mathbf{P}_i^2}{2m_1} + \sum_{j=1}^{N_2} \frac{\mathbf{p}_j^2}{2m_2}, \\ H_{11} &= \sum_{i<j}^{N_1} \phi_{11}(\mathbf{R}_{ij}), \\ H_{22} &= \sum_{i<j}^{N_2} \phi_{22}(\mathbf{r}_{ij}), \\ H_{12} &= \sum_{i=1}^{N_1} \sum_{j=1}^{N_2} \phi_{12}(\mathbf{R}_i - \mathbf{r}_j). \end{aligned} \quad (1)$$

Here m_1 and m_2 are the masses, \mathbf{P}_i and \mathbf{p}_j the linear momenta, and \mathbf{R}_i and \mathbf{r}_j the positions of the particles of species 1 and 2, respectively. The spherically symmetric pair potentials are denoted ϕ_{11} , ϕ_{22} , and ϕ_{12} , while $\mathbf{R}_{ij} = \mathbf{R}_i - \mathbf{R}_j$ and $\mathbf{r}_{ij} = \mathbf{r}_i - \mathbf{r}_j$.

At fixed inverse temperature $\beta = 1/k_B T$, the relevant thermodynamic potential of the canonical (N_1, N_2, V, T) ensemble is the Helmholtz free energy $F_c(N_1, N_2, V, T)$, given by

$$\exp[-\beta F_c] = \frac{1}{N_1! \Lambda_1^{3N_1}} \frac{1}{N_2! \Lambda_2^{3N_2}} \text{Tr}_1 \text{Tr}_2 \exp[-\beta H], \quad (2)$$

where $\Lambda_i = h/\sqrt{2\pi m_i k_B T}$ denotes the thermal wavelength of species $i = 1, 2$ as follows from the integration over the momenta. The trace Tr_1 is short for the volume integral $\int_V d\mathbf{R}^{N_1}$ over the coordinates of the particles of species 1, and similarly for Tr_2 .

It proves more convenient to consider the system in the (N_1, μ_2, V, T) ensemble, in which the chemical potential $\mu_2 = (\partial F_c / \partial N_2)_{N_1, V, T}$ of species 2 is fixed instead of the corresponding number of particles, N_2 . The associated thermodynamic potential is denoted $F(N_1, \mu_2, V, T)$, and is related to F_c by the Legendre transform

$$F(N_1, \mu_2, V) = F_c(N_1, N_2, V) - \mu_2 N_2, \quad (3)$$

where we omitted the explicit T dependence. Equivalently, we can write

$$\begin{aligned} \exp[-\beta F] &= \sum_{N_2=0}^{\infty} \exp[-\beta(F_c - \mu_2 N_2)] \\ &= \frac{1}{N_1! \Lambda_1^{3N_1}} \text{Tr}_1 \exp[-\beta(H_{11} + \Omega)], \end{aligned} \quad (4)$$

where Ω is defined in terms of the fugacity $z_2 = \Lambda_2^{-3} \exp(\beta \mu_2)$ of species 2 as

$$\exp[-\beta \Omega] = \sum_{N_2=0}^{\infty} \frac{z_2^{N_2}}{N_2!} \text{Tr}_2 \exp[-\beta(H_{12} + H_{22})]. \quad (5)$$

Note that Ω depends not only on N_1 , z_2 , and V , but also on the instantaneous coordinates \mathbf{R}_i for $i = 1, 2, \dots, N_1$ of the canonically treated component 1. In fact, the right hand side of Eq. (5) can be interpreted as the grand partition sum of a fluid of species 2 in the external field of a fixed configuration of N_1 particles of species 1. Thus we write

$$\Omega = \Omega(\{\mathbf{R}_i\}; N_1, z_2, V). \quad (6)$$

The reason why this (N_1, μ_2, V, T) ensemble is convenient can be seen from Eq. (4), as the right hand side is the canonical partition sum of a one-component system of species 1 with an effective interaction Hamiltonian

$$H^{\text{eff}} = H_{11} + \Omega. \quad (7)$$

Once Ω , and thus H^{eff} , is known for all values of z_2 , the thermodynamics and the phase behavior of the mixture can be determined from standard techniques for one-component systems. We focus therefore on the calculation of Ω . Throughout we assume the volume V to be macroscopically large.

B. Mayer expansion of Ω

In order to calculate Ω explicitly, we first introduce the Mayer functions f and g associated with the pair potentials ϕ_{12} and ϕ_{22} , respectively,

$$\begin{aligned} f_{ij} &\equiv f(\mathbf{R}_i, \mathbf{r}_j) = \exp[-\beta \phi_{12}(\mathbf{R}_i - \mathbf{r}_j)] - 1, \\ g_{kl} &\equiv g(\mathbf{r}_k, \mathbf{r}_l) = \exp[-\beta \phi_{22}(\mathbf{r}_k - \mathbf{r}_l)] - 1. \end{aligned} \quad (8)$$

In terms of these Mayer functions, we rewrite Eq. (5) as

$$\begin{aligned} \exp[-\beta \Omega] &= \sum_{N_2=0}^{\infty} \frac{z_2^{N_2}}{N_2!} \int_V d\mathbf{r}^{N_2} \prod_{i=1}^{N_1} \prod_{j=1}^{N_2} (1 + f_{ij}) \prod_{k<l}^{N_2} (1 + g_{kl}) \\ &= 1 + z_2 \int_V d\mathbf{r}_1 \prod_{i=1}^{N_1} (1 + f_{i1}) + \frac{z_2^2}{2} \int_V d\mathbf{r}_1 d\mathbf{r}_2 \\ &\quad \times \prod_{i=1}^{N_1} (1 + f_{i1})(1 + f_{i2})(1 + g_{12}) \\ &\quad + \frac{z_2^3}{3!} \int_V d\mathbf{r}_1 d\mathbf{r}_2 d\mathbf{r}_3 \prod_{i=1}^{N_1} (1 + f_{i1})(1 + f_{i2}) \\ &\quad \times (1 + f_{i3})(1 + g_{12})(1 + g_{13})(1 + g_{23}) + O(z_2^4). \end{aligned} \quad (9)$$

$$\Omega_0(z_2, V) = -Vp(z_2), \quad (16)$$

where $p(z_2)$ is the negative of the grand-potential density, or the pressure, of this one-component system.

The diagrams involving only one open big circle, representing $-\beta\Omega_1$, are recovered exactly by the identification

$$\exp[-\beta\Omega_1] = \left(\frac{\Xi_1(z_2, V)}{\Xi_0(z_2, V)} \right)^{N_1}, \quad (17)$$

where Ξ_0 is defined in Eq. (15) and where

$$\Xi_1(z_2, V) = \sum_{N_2=0}^{\infty} \frac{z_2^{N_2}}{N_2!} \int_V d\mathbf{r}^{N_2} \exp[-\beta H_{12}^{(1)}] \exp[-\beta H_{22}] \quad (18)$$

is the grand partition sum of a system of volume V consisting of a single particle of species 1 and a ‘‘sea’’ of particles of species 2 at fugacity z_2 . It follows from Eq. (17) that Ω_1 can be written as

$$\Omega_1(N_1, z_2) = N_1 \omega_1(z_2), \quad (19)$$

where ω_1 is defined by

$$\begin{aligned} \exp[-\beta\omega_1(z_2)] &= \left[\sum_{N_2=0}^{\infty} \frac{z_2^{N_2}}{N_2!} \int_V d\mathbf{r}^{N_2} \exp[-\beta H_{12}^{(1)}] \exp[-\beta H_{22}] \right] \\ &\times \left[\sum_{N_2=0}^{\infty} \frac{z_2^{N_2}}{N_2!} \int_V d\mathbf{r}^{N_2} \exp[-\beta H_{22}] \right]^{-1} \\ &\equiv \langle \exp[-\beta H_{12}^{(1)}] \rangle_{z_2}. \end{aligned} \quad (20)$$

The brackets $\langle \dots \rangle_{z_2}$ denote a statistical average in the reservoir of particles of species 2. It follows directly from Eqs. (17) and (19) that $\omega_1(z_2)$ is actually the grand-potential difference between a sea of small spheres at fugacity z_2 with and without a single particle of species 1. Another interpretation of ω_1 stems from the analogy between Eq. (20) and the Widom-insertion theorem [62]; i.e., $\omega_1(z_2)$ is seen to be a contribution to the chemical potential of species 1 due to the presence of a sea of species 2 at fugacity z_2 . This latter interpretation is, of course, consistent with the linear dependence on N_1 in Eq. (19).

It can also be shown explicitly that the exponential of the sum of connected diagrams involving two open big circles is given by

$$\exp[-\beta\Omega_2] = \prod_{i<j}^{N_1} \frac{\Xi_2(\mathbf{R}_{ij}; z_2, V) / \Xi_0(z_2, V)}{\Xi_1^2(z_2, V) / \Xi_0^2(z_2, V)}, \quad (21)$$

where Ξ_1 is given in Eq. (18) and

$$\begin{aligned} \Xi_2(\mathbf{R}_{ij}; z_2, V) &= \sum_{N_2=0}^{\infty} \frac{z_2^{N_2}}{N_2!} \int_V d\mathbf{r}^{N_2} \exp[-\beta H_{12}^{(2)}] \\ &\times \exp[-\beta H_{22}]. \end{aligned} \quad (22)$$

One recognizes that $\Xi_2(\mathbf{R}_{ij}; z_2, V)$ is the grand partition sum of a system in a volume V containing *two* particles of species 1 (at positions \mathbf{R}_i and \mathbf{R}_j) and a ‘‘sea’’ of particles of species 2 at fugacity z_2 . It follows directly from Eq. (21) that

$$\Omega_2(\{\mathbf{R}\}; N_1, z_2) = \sum_{i<j}^{N_1} \omega_2(\mathbf{R}_{ij}; z_2) \quad (23)$$

is a pairwise sum of the pair potential ω_2 defined by

$$\begin{aligned} \exp[-\beta\omega_2(\mathbf{R}_{ij}; z_2)] &= \frac{\Xi_2(\mathbf{R}_{ij}; z_2, V) / \Xi_0(z_2, V)}{\Xi_1^2(z_2, V) / \Xi_0^2(z_2, V)} \\ &= \frac{\langle \exp[-\beta H_{12}^{(2)}(\mathbf{R}_{ij})] \rangle_{z_2}}{\langle \exp[-\beta H_{12}^{(1)}] \rangle_{z_2}^2}. \end{aligned} \quad (24)$$

Arguments along the same lines yield, for the exponential of the three-body contribution Ω_3 ,

$$\exp[-\beta\Omega_3] = \prod_{i<j<k}^{N_1} \left(\frac{\Xi_3(\mathbf{R}_{i,j,k}; z_2, V)}{\Xi_0(z_2, V)} \frac{\Xi_1^3(z_2, V)}{\Xi_2(\mathbf{R}_{ij}; z_2, V) \Xi_2(\mathbf{R}_{ik}; z_2, V) \Xi_2(\mathbf{R}_{jk}; z_2, V)} \right), \quad (25)$$

where the Ξ_n for $n=0,1$, and 2 are defined in Eqs. (15), (18), and (22), and where $\Xi_3(\mathbf{R}_{i,j,k}; z_2, V)$ is the grand-canonical partition sum of the sea of species 2 at fugacity z_2 in the external field of three particles of species 1 at positions $\mathbf{R}_{i,j,k}$. It follows directly from Eq. (25) that

$$\Omega_3 = \sum_{i<j<k}^{N_1} \omega_3(\mathbf{R}_{i,j,k}; z_2), \quad (26)$$

where the three-body potential ω_3 can be rewritten in terms of the corresponding interaction Hamiltonians $H_{12}^{(n)}$ for $n=1,2,3$ as

$$\begin{aligned} \exp[-\beta\omega_3(\mathbf{R}_{i,j,k})] &= \langle \exp[-\beta H_{12}^{(3)}(\mathbf{R}_{i,j,k})] \rangle_{z_2} \\ &\times \prod_{(mn)=(ij),(ik),(jk)} \frac{\langle \exp[-\beta H_{12}^{(1)}] \rangle_{z_2}}{\langle \exp[-\beta H_{12}^{(2)}(\mathbf{R}_{mn})] \rangle_{z_2}}. \end{aligned} \quad (27)$$

In principle this process can be continued for any integer n , with the result

$$\Omega_n(\{\mathbf{R}\}; N_1, z_2) = \sum_{i_1<i_2<\dots<i_n}^{N_1} \omega_n(\mathbf{R}_{i_1, \dots, i_n}; z_2), \quad (28)$$

where the interaction ω_n between n particles of species 1 can be expressed in terms of grand-canonical averages of the Boltzmann factors associated with the Hamiltonians $H_{12}^{(m)}$ with $1 \leq m \leq n$, as we showed explicitly for $n=1,2,3$. Of course, we are still left with the problem of calculating ω_n for $n \geq 1$, but the present analysis shows that the effective Hamiltonian (7) for species 1 is of the form

$$H^{\text{eff}} = -p(z_2)V + N_1\omega_1(z_2) + \sum_{i < j}^{N_1} [\phi_{11}(\mathbf{R}_{ij}) + \omega_2(\mathbf{R}_{ij}; z_2)] \\ + \sum_{i < j < k}^{N_1} \omega_3(\mathbf{R}_{ijk}; z_2) + \dots, \quad (29)$$

where the ellipsis represents the terms Ω_n for $n \geq 4$, and where we used Eqs. (16), (19), (23), and (26).

We make four remarks on the results obtained so far. (i) We wish to emphasize that the derivation of H^{eff} holds for any two-component mixture with integrable pair interactions, and is not restricted to binary hard-sphere mixtures. The rate of convergence of the expansion of the effective Hamiltonian depends on the particular form of the pair potentials ϕ_{12} and ϕ_{22} ; one could expect a relatively fast convergence for short-ranged potentials, although correlations will generally cause the effective interactions to be longer ranged than the bare pair potentials ϕ_{12} and ϕ_{22} . (ii) As a check on the results obtained it is instructive to consider the following: $\exp[-\beta\Omega]$ is the grand-partition sum of a fluid of species 2 in the external field of a fixed configuration of N_1 particles of species 1 and the decomposition of Ω given in Eq. (13) is equivalent to the factorization $\exp[-\beta\Omega] = \prod_{n=0}^{N_1} \exp[-\beta\Omega_n]$. For $N_1=0$, i.e., no particles of species 1 in the sea of species 2, we recover from Eq. (15) that $\exp[-\beta\Omega] = \exp[-\beta\Omega_0] = \Xi_0(z_2, V)$. For $N_1=1$ we find $\exp[-\beta\Omega] = \exp[-\beta\Omega_0] \exp[-\beta\Omega_1] = \Xi_0(\Xi_1/\Xi_0) = \Xi_1$, where we used Eqs. (15) and (17). Similarly, we find, for $N_1=2$, $\exp[-\beta\Omega] = \Xi_0(\Xi_1/\Xi_0)^2(\Xi_2\Xi_0)/(\Xi_1)^2 = \Xi_2$, and for $N_1=3$ that $\exp[-\beta\Omega] = \Xi_3$. For arbitrary N_1 , we indeed find that $\exp[-\beta\Omega]$ can always be factorized into zero-, one-, two-, three-, . . . , and N_1 -body terms so that $\exp[-\beta\Omega] = \Xi_{N_1}$, as required. This scheme to factorize the partition function is actually similar in spirit to that of Ref. [63], where it is applied to a one-component imperfect gas. (iii) The terms $\Omega_0 = -p(z_2)V$ and $\Omega_1 = N_1\omega_1(z_2, V)$ that represent the zero- and one-body terms in the effective Hamiltonian (29) do not depend on the instantaneous coordinates $\{\mathbf{R}\}$ of the particles of species 1, and therefore do not affect the *structure* of the (uniform) system. Moreover, these two terms do not affect the *phase behavior* of the two-component system because of the trivial N_1 dependence or, equivalently, the trivial dependence on density $\rho_1 = N_1/V$: Ω_0/V is independent of ρ_1 , and Ω_1/V depends only linearly on ρ_1 . Since two coexisting phases must have the same chemical potential of species 2, and hence the same z_2 , the two terms under consideration do not affect the common tangent constructions, as explained further in the Appendix. This innocuous character of Ω_0 and Ω_1 is to be contrasted with analogous terms for systems with long-ranged Coulomb interactions, for which the Mayer expansion diverges so that the present derivation does not apply directly. Recently, it

was shown [64,65] that a system of charged colloids suspended in a solvent with coions and counterions can be mapped onto an effective one-component colloidal system by integrating out the degrees of freedom of the coions and counterions. The usual Derjaguin-Landau-Verwey-Overbeek (screened-Coulomb) potential was recovered for the two-body term, as expected. However, the charge neutrality constraint gives a nontrivial dependence of the one-body term on the colloid density which has dramatic consequences for the phase behavior at low salt concentrations [64,65]. (iv) We see from Eq. (24) that $\omega_2(\mathbf{R}_{ij}; z_2)$ is the grand-potential difference between the sea, of fugacity z_2 , containing two particles of species 1 at a finite separation \mathbf{R}_{ij} and at infinite separation $\mathbf{R}_{ij} = \infty$. In other words ω_2 is the work done in bringing a particle of species 1 from infinity, but still in the reservoir of fixed z_2 , to a finite distance from another particle of species 1 located at the origin.

IV. APPLICATION TO A BINARY MIXTURE OF HARD SPHERES

In the previous section we showed that we can describe a classical binary fluid by an effective one-component Hamiltonian [Eq. (29)]. In this section we apply this approach to the particular case of a mixture of large and small hard spheres with diameters σ_1 and σ_2 , respectively. The size ratio is denoted $q = \sigma_2/\sigma_1 \leq 1$. The pair potentials $\phi_{ij}(r)$ are the usual additive hard-sphere potentials, i.e., infinite for $0 < r < (\sigma_i + \sigma_j)/2$ and zero otherwise. The zeroth-order term Ω_0 is equal to the grand potential of a pure system of small hard spheres at fugacity z_2 :

$$\Omega_0(z_2, V) = -Vp_{\text{hs}}(z_2), \quad (30)$$

where $p_{\text{hs}}(z_2)$ is the pressure of the small hard-sphere system. This pressure is accurately described by the Carnahan-Starling equation of state for the fluid state values of z_2 of interest. An explicit scaled particle expression for $\omega_1(z_2)$ is given by Henderson, and consists of a volume, a surface, and a σ_1 -independent term $K(z_2)$ [66]:

$$N_1\omega_1(z_2) = p_{\text{hs}}(z_2)V\eta_1(1+q)^3 + \gamma_{\text{hs}}(z_2, R_1)\pi\sigma_1^2N_1 \\ + K(z_2)N_1, \quad (31)$$

where $\gamma_{\text{hs}}(z_2, R_1)$ is the surface tension of a hard-sphere fluid at a hard-spherical wall with a radius $R_1 = \sigma_1/2$, and $\eta_1 = \pi\sigma_1^3N_1/6V$ is the large-sphere packing fraction [67]. The two-body term Ω_2 can be written as a sum of pair potentials ω_2 ; see Eq. (23). In the case of hard spheres this pair potential can be identified with the depletion potential:

$$\omega_2(\mathbf{R}_{ij}; z_2) = \phi_{\text{dep}}(R_{ij}; z_2). \quad (32)$$

Attard [50] has derived an exact expression for the depletion *force* between two large spheres and this has been employed in simulation studies of depletion [51]. Recently, Mao *et al.* calculated the depletion potential within the Derjaguin approximation up to third order in η_2^r , and found excellent agreement with simulations for $q=0.1$ and for η_2^r as large as 0.34 [52,53]. Here η_2^r is the packing fraction of a reservoir of small hard spheres at fugacity z_2 . In this work, we use the

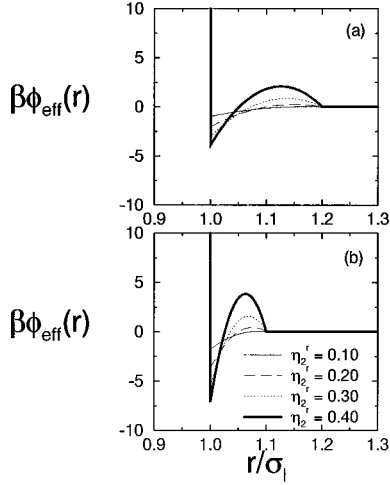


FIG. 1. The effective large-sphere pair potential, i.e., the sum of the depletion potential (33) and the large hard-sphere potential ϕ_{11} , of a binary hard-sphere mixture with size ratio (a) $q=0.2$ and (b) $q=0.1$, for several small-sphere reservoir packing fractions η_2^r .

simpler expression given by Götzelmann *et al.* which, up to third order in η_2^r , is equally accurate and reads [54]

$$\beta\phi_{\text{dep}}(R_{ij}) = -\frac{1+q}{2q} [3x^2\eta_2^r + (9x+12x^2)(\eta_2^r)^2 + (36x+30x^2)(\eta_2^r)^3] \quad \text{for } -1 < x < 0, \quad (33)$$

where $x = R_{ij}/\sigma_2 - 1/q - 1$. Contact corresponds to $R_{ij} = \sigma_1$ or $x = -1$. The total effective pair potential is from Eq. (29):

$$\phi_{\text{eff}} = \phi_{11} + \phi_{\text{dep}}, \quad (34)$$

where ϕ_{11} is the bare hard-sphere potential between two large spheres. Examples of ϕ_{eff} are shown in Fig. 1 for size ratios $q=0.2$ and 0.1 at several values of reservoir packing fraction η_2^r . This pair potential contains a deep and narrow potential well close to the surface of the large sphere, followed by a small repulsive barrier. The range of the potential is equal to q times the large sphere diameter. For simplicity (see [54]) we set $\phi_{\text{dep}} = 0$ for $R_{ij} > \sigma_1 + \sigma_2$, and thus we neglect longer-ranged and weaker oscillations; we expect these to be unimportant for the phase behavior of the mixture. It is worthwhile noting that exact expressions for the depletion potential were given in Ref. [54] within the context of the Derjaguin approximation. However, these expressions give a poor account of the simulation results of Ref. [53] for $q=0.1$ and $\eta_2^r > 0.3$, thereby casting doubts on the validity of the Derjaguin approximation for these values of q and η_2^r .

In all our effective one-component calculations we set $\Omega_n = 0$ for $n \geq 3$. This approximation was tested for $q=0.1$ in computer simulations by Biben *et al.*, who found that the three-body term, denoted ω_3 above, contributes less than 0.5% at $\eta_2^r \approx 0.3$ [53]. The neglect of ω_3 can be made plausible by geometric arguments for $q < 0.154$, since then three or more nonoverlapping large spheres cannot simultaneously overlap with a small one; i.e., the first and dominant diagram in the three-body term Ω_3 vanishes. However, it is important

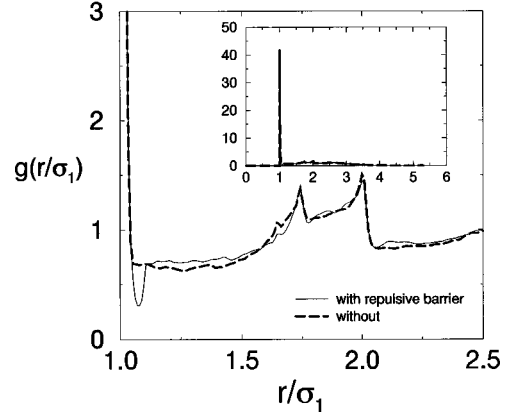


FIG. 2. The radial distribution function $g(r/\sigma_1)$ for the effective one-component system with packing fractions $\eta_1=0.35$, $\eta_2^r=0.25$, and $q=0.1$ calculated using the depletion potential (33) with and without the small repulsive barrier. Note that this state point falls well inside the fluid-solid coexistence region [see Fig. 4(b)].

to realize that other diagrams in Ω_3 are not necessarily zero, even for $q < 0.154$, so that the neglect of all three-body and higher-body terms is an approximation. At this stage it is not evident that q plays the (formal) role of a small parameter.

Thus we arrive at the effective one-component Hamiltonian

$$H^{\text{eff}} = H_0 + \sum_{i < j}^{N_1} \phi_{\text{eff}}(R_{ij}), \quad (35)$$

where, as mentioned in Sec. III,

$$H_0 = -p_{\text{hs}}(z_2) [1 - \eta_1(1+q)^3] V + \gamma_{\text{hs}}(z_2, R_1) \pi \sigma_1^2 N_1 + K(z_2) N_1 \quad (36)$$

is irrelevant for the phase behavior of the fluid, and where ϕ_{eff} is defined in Eq. (34). We have now mapped the binary hard-sphere mixture onto an (approximate) effective one-component system of large spheres, which can be treated with standard techniques.

V. RESULTS OF SIMULATIONS OF THE EFFECTIVE HAMILTONIAN

A. Phase diagram

At first sight, one might think that the phase behavior of the effective one-component system characterized by Eqs. (34) and (35) can be determined by standard perturbation theory using the pure hard-sphere system at the same packing fraction as a reference system. Using first-order perturbation theory for $q=0.1$, we did not find any indication of a fluid-fluid spinodal for packing fractions $\eta_1 < 0.5$. This result was also found in Ref. [54]. However, our simulations of the system described by ϕ_{eff} given in Eq. (34) yield radial distribution functions $g(r)$ that differ enormously from those of the reference hard-sphere fluid at the same η_1 . This is illustrated in Fig. 2, where we plot $g(r)$ for $\eta_1=0.35$, $\eta_2^r=0.25$, and $q=0.1$. We find that $g(\sigma_1) \approx 42$, which should be compared with the much lower contact value ≈ 3 for the hard-sphere reference system. Similar large contact values,

which may signal a strong tendency for clustering, have been observed in previous simulation and integral equation studies [53,68], and also in experiments on colloidal hard-sphere mixtures [69]. The enormous difference between $g(r)$ of the reference hard-sphere system and that of the effective system signals the breakdown of perturbation theory, and thus we resort to full numerical simulations for the free energy F of the effective system.

Before describing these simulations we compare $g(r)$ for a depletion potential with and without the repulsive barrier. Figure 2 shows that the contact value and most other structural features are not sensitive to the repulsive barrier, apart from a small well near $r=1.07\sigma_1$, which does reflect the presence of the barrier. We conclude that small differences in the choice of depletion potential—such as our omission of the very weak oscillations for $R_{ij} > (\sigma_1 + \sigma_2)$ —should not have a drastic effect on the resulting phase equilibria. It probably suffices to have a good account of the potential well close to contact, while the first repulsive barrier, as well as the longer-ranged oscillations, should play only a minor role. Note that the peaks in $g(r)$ near $r/\sigma_1 = 1.74$ and 2.0 are similar to those found at state point ‘‘C’’ of Ref. [53] where it is argued that these arise from a particular local organization of particles equivalent to that in the sticky-sphere model.

In order to determine the phase diagram of the effective one-component system, we first calculate the thermodynamic potential F , defined in Eq. (4), as a function of N_1 , V , and z_2 . We actually determine the dimensionless free energy density $f = (\pi/6)\sigma_1^3 F/V$ as a function of η_1 and z_2 . For convenience we often replace the dependence on z_2 by that on the reservoir packing fraction η_2^r . As the free energy cannot be measured directly in a Monte Carlo (MC) simulation, we use thermodynamic integration to relate the free energy of the effective system to that of a reference hard-sphere system at the same large-sphere packing fraction η_1 . To this end we introduce the auxiliary effective Hamiltonian

$$H_\lambda^{\text{eff}} = \sum_{i<j}^{N_1} [\phi_{11}(R_{ij}) + \lambda \phi_{\text{dep}}(R_{ij})], \quad (37)$$

where $0 \leq \lambda \leq 1$ is a dimensionless coupling parameter: at $\lambda=0$ the auxiliary Hamiltonian is that of the pure system of N_1 large hard spheres, while at $\lambda=1$ it is the effective Hamiltonian of interest (for fixed z_2 and V). It is a standard result [70–72] that

$$F(N_1, V, z_2) = F(N_1, V, z_2=0) + \int_0^1 d\lambda \left\langle \sum_{i<j}^{N_1} \phi_{\text{dep}}(R_{ij}) \right\rangle_{N_1, V, z_2, \lambda}, \quad (38)$$

where $F(N_1, V, z_2=0)$ is the free energy of the pure reference system of large hard spheres ($\lambda=0$), for which we use the Carnahan-Starling expressions [73] for the fluid, and the analytic form for the equation of state proposed by Hall [74] for the solid phase. In the latter case an integration constant is determined such that the known fluid-solid coexistence of the pure hard-sphere system is recovered [11]. The angular brackets $\langle \dots \rangle_{N_1, V, z_2, \lambda}$ denote a canonical average over the system of N_1 particles interacting via the auxiliary Hamil-

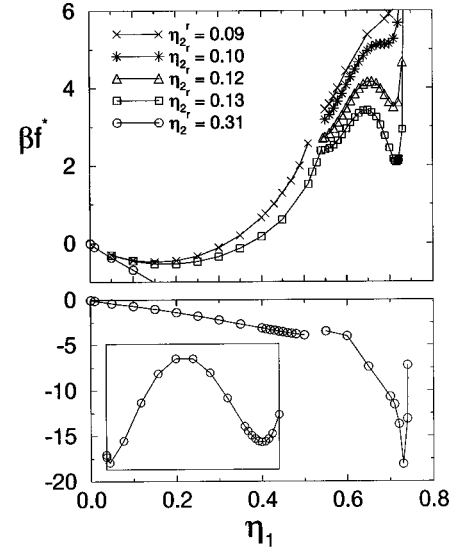


FIG. 3. Reduced free energy $\beta f^* = \beta[F - (\Omega_0 + \Omega_1)]\sigma_1^3/V$ versus η_1 for $q=0.1$ at several η_2^r . The curves for $\eta_1 \geq 0.54$ are the solid branches, while the curves for lower η_1 are the fluid branches. Note the difference in scale for $\eta_2^r = 0.31$. For clarity, we subtracted a linear fit in η_1 to the data for $\eta_2^r = 0.31$ (see inset). For a given η_2^r common tangent constructions can be made to determine the values of η_1 at coexistence.

tonian H_λ^{eff} . The integrand in Eq. (38) can, for a fixed λ , be measured in a standard MC calculation; for the numerical λ integration, we use a ten-point Gauss-Legendre quadrature [75].

In order to map out the phase diagram $f(\eta_1, z_2)$ must be determined from λ integrations for many state points (η_1, z_2) . We chose therefore to simulate relatively small systems, with $N_1 = 108$. As an illustration we plot, in Fig. 3, f as a function of η_1 at several η_2^r for $q=0.1$. For $\eta_2^r > 0.06$ we find that the solid branch of f becomes nonconvex, indicative of a spinodal instability. For $\eta_2^r > 0.29$ another spinodal instability is found, but now in the fluid branch. This instability can be seen clearly in the inset of Fig. 3, where f is shown at $\eta_2^r = 0.31$. For clarity, we have subtracted a linear fit in η_1 , which does not affect the common tangent construction. Note that each point in the (η_1, η_2^r) plane is obtained by an independent λ integration. In order to construct the full phase diagram we employ common tangent constructions at fixed z_2 to obtain the coexisting phases. We fitted polynomials to f and computed the pressure and chemical potential at each η_1 . The densities of the coexisting phases can then be determined by equating the pressures and chemical potentials in both phases. For more details we refer the reader to the Appendix.

The above procedure has been carried out to determine the phase diagram for size ratios $q=0.2, 0.1, 0.05$, and 0.033 . In Fig. 4, we show the resulting phase diagrams in the (η_1, η_2^r) plane. This representation, which is the natural one given our approach, implies that the tie lines connecting coexisting state points are horizontal. The shaded areas represent the (metastable) fluid-fluid and solid-solid two-phase regions. At $\eta_2^r = 0$ and for all q we recover the known freezing transition of the pure hard-sphere system.

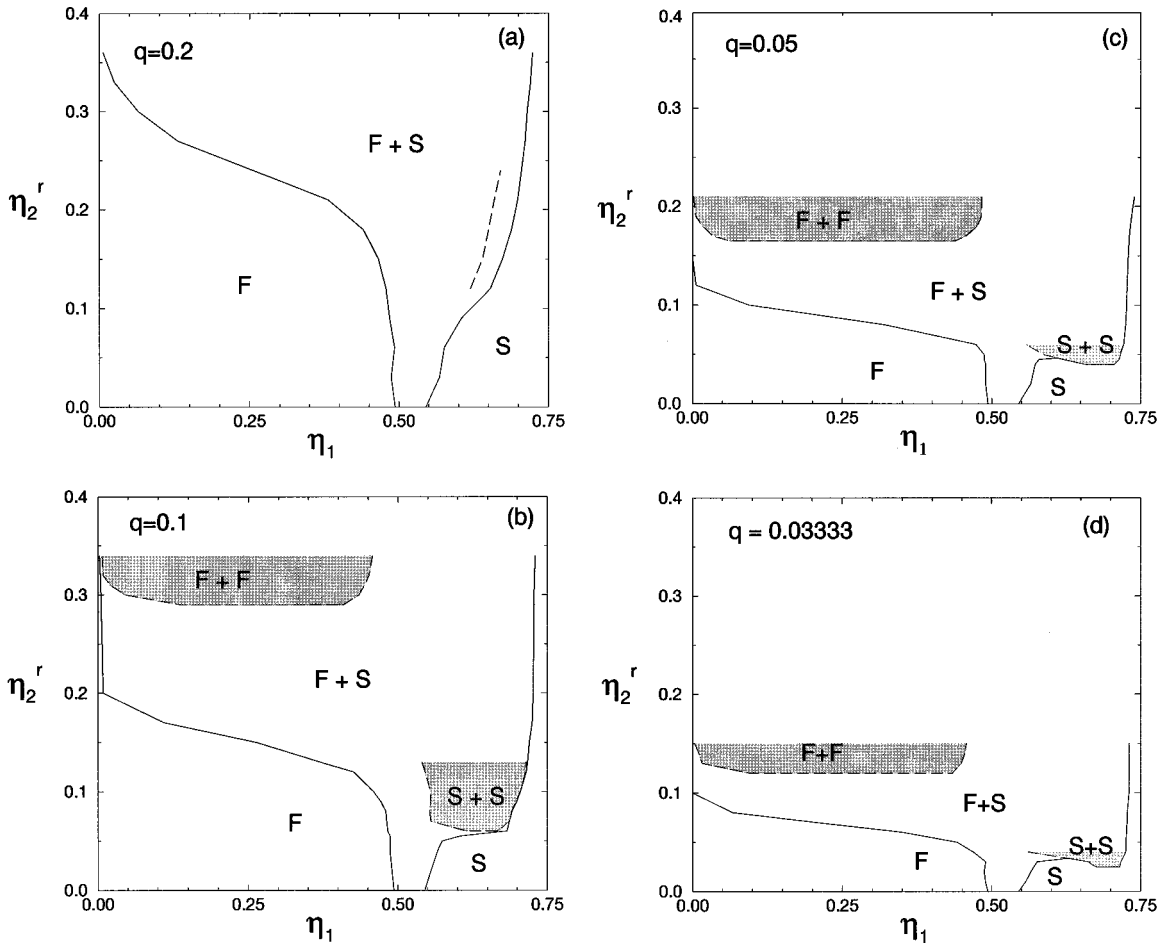


FIG. 4. Phase diagram of binary hard-sphere mixtures with size ratios (a) $q=0.20$, (b) $q=0.10$, (c) $q=0.05$, and (d) $q=0.033$ as a function of the large-sphere packing fraction η_1 and the small sphere reservoir packing fraction η_2^r as obtained from simulations of the effective one-component Hamiltonian. F and S denote the stable fluid and solid (fcc) phase. $F+S$, $F+F$, and $S+S$ denote, respectively, the stable fluid-solid, the metastable fluid-fluid, and the solid-solid coexistence regions. The dashed line in (a) denotes the spinodal instability on the solid branch. Note that the solid-solid coexistence for $q \leq 0.05$ becomes stable and that all the tie lines are horizontal (not drawn).

For $q \leq 0.2$, an enormous widening of the fluid-solid transition is observed when η_2^r increases sufficiently. This implies that the coexisting fluid and solid phases become progressively more dilute and dense, respectively, upon increasing η_2^r . This widening is consistent with findings by Gast *et al.* [61] in perturbation theory studies of the Asakura-Oosawa depletion potential model [30,31], and has also been observed in experiments on colloid mixtures, where small amounts of small spheres induce a rapid decrease in the lattice constant of the crystal [39]. The shape of the coexistence curve for $\eta_2^r > 0.1$ implies that the fluid phase only persists to very low values of η_1 .

The calculations also reveal the existence of a fluid-fluid transition for $q \leq 0.1$. However, this fluid-fluid coexistence is metastable with respect to the broad fluid-solid transition for all q and η_2^r . It is of interest to note that for all $q \leq 0.1$ the critical point of the metastable fluid-fluid coexistence curve occurs at a value of η_2^r that is about twice that of the fluid-solid curve at the same η_1 . Thus the fluid-fluid curve does *not* move deeper into the fluid-solid coexistence region upon decreasing q , i.e., upon decreasing the range of the potential. This situation is in contrast to the findings of Ref. [71] where for a Yukawa pair potential decreasing the range of the attraction lowers, in temperature, the fluid-fluid coexistence

into the fluid-solid region. Here there is no trend that suggests a stable fluid-fluid curve at $q < 0.033$. For $q=0.2$ we do not find a spinodal instability in the fluid branch for $\eta_2^r < 0.46$, while we do find a spinodal instability in the solid branch for $\eta_2^r > 0.12$. However, in Fig. 5 we show that as soon as the spinodal instability appears in the solid phase, this instability is very broad and disappears in the fluid phase. We were not able therefore to find a metastable solid-solid coexistence using the common-tangent construction. Rather, we plot in Fig. 4(a) the spinodal (dashed curve) which is given by $(\partial^2 f / \partial \eta_1^2) = 0$. The presence of this spinodal instability on the solid branch may be important for the kinetics of the phase separation of the mixture [36,76].

More surprisingly perhaps, the phase diagrams also show the existence of an isostructural solid-solid transition for $q \leq 0.1$. For $q=0.1$, the solid-solid coexistence region is found to be metastable with respect to the freezing transition, although the critical point of the solid-solid binodal is very close to the stable fluid-solid phase boundary. For smaller q the most striking feature is the downward shift of the solid-solid with respect to the fluid-solid binodal, so that there is a regime with a stable solid-solid coexistence for $q \leq 0.05$. Simultaneously, the solid-solid critical point shifts closer to close packing upon decreasing q . These results are consistent

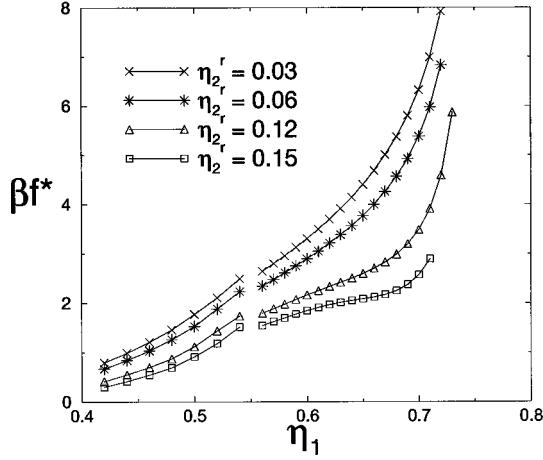


FIG. 5. Reduced free energy $\beta f^* = \beta[F - (\Omega_0 + \Omega_1)]\pi\sigma_1^3/6V$ versus η_1 for $q=0.2$ at several η_2^r . The curves for $\eta_1 \geq 0.54$ are the solid branches, while the curves for lower η_1 are the fluid branches.

with those of Refs. [72,77] for square-well and Yukawa fluids, where the authors find a solid-solid transition when the range of the potential is sufficiently short. The coexisting densities for $q=0.2, 0.1, 0.05$, and 0.033 are tabulated in Tables I, II, III, and IV.

Within the context of the Percus-Yevick approximation, it has been shown that the binary hard-sphere mixture in the limit of $q \rightarrow 0$ is equivalent to the one-component Baxter sticky-sphere model [78]. The latter is obtained from the square-well model by considering the limit $\delta/\sigma_1 \rightarrow 0, \beta\epsilon \rightarrow \infty$ with $\tau = (1/12)(\sigma_1/\delta)\exp[-\beta\epsilon]$ finite, where ϵ and δ are the well depth and the well width, respectively. Note that τ plays the role of a dimensionless nonlinear temperature. In the (η_1, τ) plane the sticky (or adhesive) hard-sphere model exhibits a vertical solid-solid binodal at close packing for τ infinite, while for any finite τ it exhibits a coexistence between a close-packed solid and an infinitely dilute gas, with all other phases at best metastable and probably unstable [72]. This pathological behavior of the adhesive hard-sphere

TABLE I. The coexisting densities (expressed in terms of the packing fraction η_1 of the large spheres) at the fluid-solid transition for a binary mixture of hard spheres with size ratio $q=0.2$ and varying packing fractions η_2^r of small spheres in the reservoir as obtained from simulations with the effective Hamiltonian.

Fluid-solid		
η_2^r	η_1 (fluid)	η_1 (solid)
0.00	0.494	0.545
0.03	0.487	0.568
0.06	0.492	0.576
0.09	0.484	0.605
0.12	0.478	0.653
0.15	0.466	0.673
0.18	0.440	0.689
0.21	0.381	0.699
0.27	0.131	0.711
0.30	0.0652	0.715
0.33	0.0252	0.720
0.36	0.00639	0.724

TABLE II. The coexisting densities at the fluid-solid, solid-solid, and fluid-fluid transitions for a binary mixture of hard spheres with size ratio $q=0.1$ and varying packing fractions η_2^r of small spheres in the reservoir as obtained from simulations with the effective Hamiltonian.

Fluid-solid		
η_2^r	η_1 (fluid)	η_1 (solid)
0.00	0.494	0.545
0.02	0.491	0.555
0.04	0.487	0.567
0.05	0.487	0.574
0.055	0.487	0.605
0.06	0.483	0.683
0.08	0.480	0.692
0.09	0.472	0.700
0.10	0.459	0.706
0.12	0.426	0.715
0.13	0.370	0.718
0.15	0.264	0.720
0.17	0.110	0.725
0.20	0.00863	0.727
0.31	0.00424	0.728
0.34	0.00274	0.730
Solid-solid		
η_2^r	η_1 (solid 1)	η_1 (solid 2)
0.06	0.613	0.669
0.07	0.556	0.687
0.08	0.553	0.691
0.09	0.555	0.698
0.10	0.555	0.705
0.12	0.546	0.714
0.13	0.541	0.715
Fluid-fluid		
η_2^r	η_1 (fluid 1)	η_1 (fluid 2)
0.29	0.140	0.408
0.30	0.0461	0.435
0.31	0.0207	0.444
0.32	0.00874	0.452
0.34	0.00672	0.458

model is consistent with Stell's analysis of the 12th virial coefficient, which was shown to be divergent [79]. It follows from Eq. (33) that the depletion potential for $q \rightarrow 0$ and $\eta_2^r > 0$ gives rise to a well depth $\beta\epsilon \sim \eta_2^r/q$, to a well width $\delta/\sigma_1 \sim q$, and hence to $\tau \sim (1/q)\exp[-\eta_2^r/q]$ where we neglect irrelevant terms of order unity. Under the condition that $\eta_2^r > q \ln(1/q^{(1+\psi)})$ and $\psi > 0$, this gives rise to $\tau \rightarrow 0$ for $q \rightarrow 0$, i.e., to the "ground state" of the adhesive hard-sphere model. If, however, η_2^r is taken so small that $\eta_2^r < q \ln(1/q^{(1+\psi)})$ for $q \rightarrow 0$, then the high-temperature limit $\tau \rightarrow \infty$ is obtained, corresponding to the one-component hard-sphere system with its "normal" hard-sphere freezing transition. One can thus envisage two different $q \rightarrow 0$ limiting procedures: (i) the Baxter-like limit in which τ is nonzero by

TABLE III. The coexisting densities at the fluid-solid, solid-solid, and fluid-fluid transitions for a binary mixture of hard spheres with size ratio $q=0.05$ and varying packing fractions η_2^r of small spheres in the reservoir as obtained from simulations with the effective Hamiltonian.

Fluid-solid		
η_2^r	η_1 (fluid)	η_1 (solid)
0.00	0.494	0.545
0.02	0.490	0.566
0.04	0.490	0.573
0.045	0.487	0.580
0.05	0.487	0.717
0.06	0.473	0.722
0.08	0.320	0.726
0.10	0.093	0.727
0.12	0.0061	0.728
0.15	1.75×10^{-4}	0.730
0.17	4.94×10^{-6}	0.731
0.19	3.30×10^{-7}	0.735
0.21	2.30×10^{-7}	0.740
Solid-solid		
η_2^r	η_1 (solid 1)	η_1 (solid 2)
0.04	0.658	0.707
0.045	0.619	0.715
0.05	0.587	0.717
0.06	0.558	0.722
Fluid-fluid		
η_2^r	η_1 (fluid 1)	η_1 (fluid 2)
0.165	0.0622	0.437
0.17	0.0540	0.447
0.18	0.0170	0.475
0.19	0.0058	0.483

restricting attention to sufficiently small η_2^r or (ii) the Stell-like so-called β_0 limit where η_2^r is fixed resulting in $\tau=0$ unless $\eta_2^r=0$ [79]. It is the latter procedure that is relevant for a comparison with the limiting $q \rightarrow 0$ behavior of binary hard-sphere mixtures. The resulting phase diagram, in the (η_1, η_2^r) plane, of the effective one-component system with an infinitesimal q is shown in Fig. 6. There is a vertical solid-solid binodal at close packing in the limit $\eta_2^r \rightarrow 0$. However, for all $\eta_2^r > 0$ the phase diagram shows coexistence between a close-packed solid and an infinitely dilute gas, while all other phases are metastable [72]. Clearly, all trends as a function of q featured in Fig. 4 are consistent with the fact that the phase diagram approaches that of the adhesive hard-sphere model in Stell's double limit $q \rightarrow 0$ and $\eta_2^r \rightarrow 0$.

In order to test the range of validity of the depletion potential picture, we also studied the extreme limit of $q=1$, where the system of "large" spheres (species 1) is in equilibrium with a reservoir of "small" spheres (species 2) which have exactly the same diameter and a packing fraction η_2^r . The depletion potential (33) is based on the Derjaguin approximation which becomes exact in the limit $q=0$, but

TABLE IV. The coexisting densities at the fluid-solid, solid-solid, and fluid-fluid transitions for a binary mixture of hard spheres with size ratio $q=0.033$ and varying packing fractions η_2^r of small spheres in the reservoir as obtained from simulations with the effective Hamiltonian.

Fluid-solid		
η_2^r	η_1 (fluid)	η_1 (solid)
0.00	0.494	0.545
0.01	0.489	0.557
0.02	0.488	0.566
0.03	0.489	0.576
0.04	0.469	0.725
0.05	0.442	0.726
0.06	0.349	0.727
0.07	0.205	0.728
0.08	0.06695	0.729
0.10	8.816×10^{-5}	0.731
0.15	0.00	0.733
Solid-solid		
η_2^r	η_1 (solid 1)	η_1 (solid 2)
0.025	0.676	0.7159
0.028	0.666	0.7164
0.03	0.664	0.7175
0.04	0.562	0.7253
Fluid-fluid		
η_2^r	η_1 (fluid 1)	η_1 (fluid 2)
0.12	0.0943	0.434
0.13	0.0161	0.449
0.14	0.0108	0.455
0.15	0.004	0.457

cannot be expected to be accurate for $q \rightarrow 1$. In the limit $q=1$, the actual depletion potential between two hard spheres suspended in a fluid of hard spheres with exactly the same diameter is given by $-k_B T \ln[g(r)]$, i.e., the potential of mean force [54]. We therefore computed $g(r)$ in a simulation for a system of pure hard spheres at a packing fraction η_2^r . In Fig. 7, we compare the depletion potential (33) with $-k_B T \ln[g(r)]$ for $\eta_2^r=0.1, 0.2$, and 0.3 . There is reasonably good agreement except in the repulsive barrier for $\eta_2^r=0.3$. We then performed simulations of the effective one-component system interacting with the depletion potential (33) for $q=1$. Figure 8 shows that the fluid-solid coexistence hardly varies with η_2^r and remains narrow. This phase diagram agrees rather well with the theoretical prediction represented by the dashed curve. The latter is obtained by equating the pressure and the chemical potential of species 1 in the solid and fluid phases and by equating the chemical potential of species 2 to that of the reservoir. This amounts to solving the four equations

$$\beta P_{\text{Hall}}(\eta^{\text{solid}}) = \beta P_{\text{CS}}(\eta^{\text{fluid}}),$$

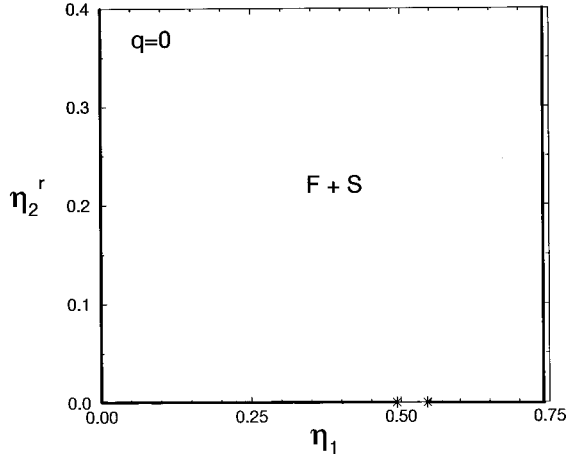


FIG. 6. Phase diagram of binary hard-sphere mixtures for an extremely small but nonzero size ratio q , based on the effective one-component Hamiltonian, plotted as a function of the large-sphere packing fraction η_1 and the small-sphere reservoir packing fraction η_2^r . For $\eta_2^r=0$, the only transition is the freezing transition of pure hard spheres denoted by two asterisks. For $\eta_2^r>0$ a very broad freezing transition is found, corresponding to coexistence of an infinitely dilute fluid ($\eta_1=0$) and a close-packed solid ($\eta_1 \approx 0.7404$). In addition, an infinitesimally narrow solid-solid transition exists at close packing for $\eta_2^r>0$.

$$\begin{aligned} \ln \eta_1^{\text{solid}} + \beta \mu_{\text{Hall}}^{\text{ex}}(\eta^{\text{solid}}) &= \ln \eta_1^{\text{fluid}} + \beta \mu_{\text{CS}}^{\text{ex}}(\eta^{\text{fluid}}), \\ \beta \mu_2 &= \ln \eta_2^{\text{solid}} + \beta \mu_{\text{Hall}}^{\text{ex}}(\eta^{\text{solid}}), \\ \beta \mu_2 &= \ln \eta_2^{\text{fluid}} + \beta \mu_{\text{CS}}^{\text{ex}}(\eta^{\text{fluid}}), \end{aligned}$$

for the four unknowns $\eta_{1,2}^{\text{fluid}}$, and $\eta_{1,2}^{\text{solid}}$ with $\eta^{\text{fluid}} = \eta_1^{\text{fluid}} + \eta_2^{\text{fluid}}$ and $\eta^{\text{solid}} = \eta_1^{\text{solid}} + \eta_2^{\text{solid}}$ for fixed values of μ_2 . The theoretical result should be near exact since the very accurate Carnahan-Starling and Hall expressions for the pressure and excess chemical potentials in the fluid and solid phase, respectively, are used. Note that the excess chemical potential

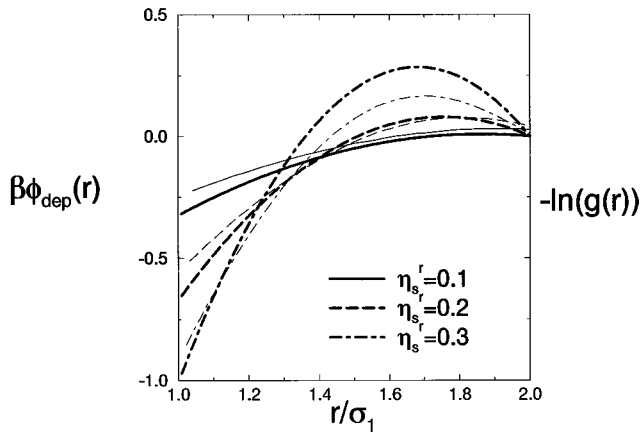


FIG. 7. The depletion potential (33) of a binary hard-sphere mixture with size ratio $q=1.0$ and small-sphere reservoir packing fractions $\eta_2^r=0.10$ (thick solid line), 0.20 (thick dashed line), and 0.30 (thick dash-dotted line). The thin lines denote $-\ln[g(r)]$ of a system of pure hard spheres at a packing fraction $\eta=0.10$ (thin solid line), 0.20 (thin dashed line), and 0.30 (thin dash-dotted line).

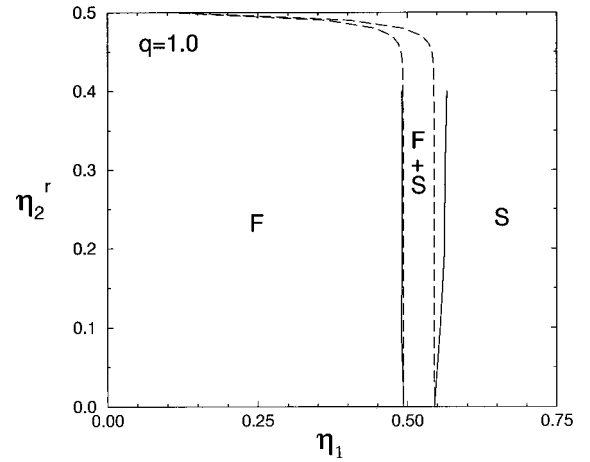


FIG. 8. Phase diagram of binary hard-sphere mixtures with size ratio $q=1.0$, based on the effective one-component Hamiltonian, plotted as a function of the large-sphere packing fraction η_1 and the small-sphere reservoir packing fraction η_2^r . The dashed lines denote the theoretical phase boundaries—see text.

μ^{ex} and the pressure P depend only on the total packing fraction η^{fluid} and η^{solid} . The ideal gas contributions to the chemical potentials take into account the distinguishability of the two species; the total chemical potential of the ‘‘small’’ spheres in the system is dictated by that of the reservoir, i.e., μ_2 . The good agreement between the theoretical phase diagram and the one based on the depletion potential for $\eta_2^r \leq 0.4$ is indicative of the good performance of depletion potentials, even in regimes where one could expect the depletion picture to fail. In Sec. VI we reconfirm this remark. The sharp bending of the theoretical fluid-solid phase boundary towards low η_1 for $\eta_2^r \geq 0.45$ can be understood if one realizes that the state point $(\eta_1, \eta_2^r) = (0, 0.494)$ is the end point of both curves, i.e., where the reservoir freezes.

B. Structure

The structure of hard-sphere mixtures has been studied extensively by integral equation theories and by simulations [80]. Here we present results for the radial distribution function $g(r)$ and the structure factor $S(k)$ obtained from simulations with $N_1 = 1000$ large spheres, interacting with the effective pair potential given by Eqs. (33) and (34), i.e., the same pair potential used to calculate the phase diagrams. In Fig. 9 we show $g(r)$ for $q=0.1$ at several values of η_2^r for (a) $\eta_1=0.05$, (b) $\eta_1=0.10$, (c) $\eta_1=0.20$, and (d) $\eta_1=0.30$. At each η_1 we find the following features for increasing η_2^r : (i) the contact value of $g(r)$ increases, (ii) the minimum near $r=1.07\sigma_1$ becomes more pronounced as the repulsive barrier grows, and (iii) the peak at $r/\sigma_1=2$ becomes more pronounced. Similar results were found in integral equation theories and simulation studies of the true binary hard-sphere mixture [53,68,80]. Comparing the state points considered in Fig. 9 with the phase diagrams plotted in Fig. 4(b), we find that the fluid-solid binodal is crossed, for each η_1 , as η_2^r is increased between 0.15 and 0.20. There is, however, *no* clear signature of this freezing transition in $g(r)$. As the coexistence line is crossed the form of $g(r)$ obtained from the simulations does not change discontinuously. This would seem to

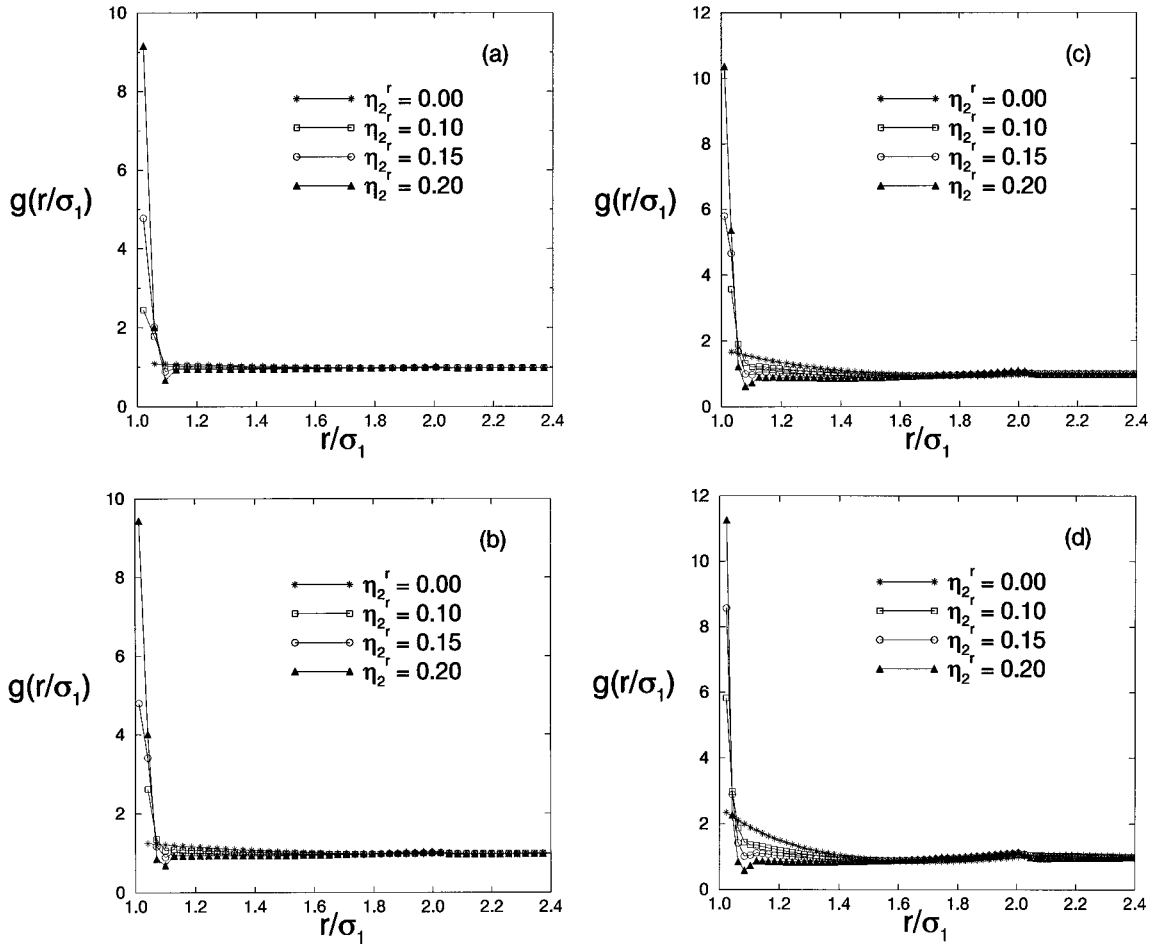


FIG. 9. The radial distribution function $g(r/\sigma_1)$ for the effective one-component system, based on the depletion potential (33) with size ratio $q=0.1$, small-sphere reservoir packing fractions $\eta_2^r=0.00, 0.10, 0.15$, and 0.20 , and with large-sphere packing fractions (a) $\eta_1=0.05$, (b) $\eta_1=0.10$, (c) $\eta_1=0.20$, and (d) $\eta_1=0.30$. In each case the states with $\eta_2^r=0.20$ lie in the solid-fluid coexistence region. In (d) the state with $\eta_2^r=0.15$ is just inside this coexistence region.

preclude using the form of the simulated $g(r)$ as a criterion to determine freezing in binary mixtures. In the thermodynamic limit $g(r)$ in the two-phase region would be the concentration-weighted sum of the radial distribution functions of the coexisting fluid and solid phases. However, the nature of $g(r)$ obtained from finite simulations in a two-phase region depends on several factors making its interpretation rather complicated. Note that the peak near $r=1.73\sigma_1$ found in Fig. 2 (at $\eta_1=0.35$, $\eta_2^r=0.25$) is not present at the state points investigated in Fig. 9. It appears that this particular feature only develops deep inside the two-phase region.

The structure factor $S(k)$ is shown in Fig. 10 for the same state points. This was calculated directly, using $S(k) = N^{-1} \langle \rho(\mathbf{k}) \rho(-\mathbf{k}) \rangle$, where $\rho(\mathbf{k}) = \sum_{i=1}^{N_1} \exp(i\mathbf{k} \cdot \mathbf{R}_i)$. For each η_1 considered we observe an increase of the (extrapolated) value of $S(k=0)$ with increasing η_2^r . An increase of $S(k=0)$ was also found in experiments on hard-sphere colloid mixtures [69] and in other simulations of binary hard-sphere mixtures based on effective pair potentials [53]. As η_2^r is increased the depletion potential becomes more attractive; i.e., the well deepens, and simple random phase approximation (RPA) arguments indicate that $S(k=0)$ should then increase—provided the repulsive barrier does not be-

come too large [54]. For the most dilute system $\eta_1=0.05$, $S(k)$ is monotonically increasing with k at small k for $\eta_2^r \leq 0.15$ but for $\eta_2^r=0.20$ —a point in the fluid-solid coexistence region—there is pronounced small-angle scattering [an increase of $S(k)$ as $k \rightarrow 0$] which reflects the growth of dense clusters of the large spheres. For higher values of η_1 again we do not observe this increase of $S(k)$ at small k until we enter the two-phase region. However, when this occurs the structure factor becomes quite noisy.

Another significant feature which is observed within the single (fluid) phase is that k_m , the position of the first peak in $S(k)$, shifts to values that are higher than the value for pure hard spheres as η_2^r is increased at fixed η_1 . This seems to be a feature of potentials with short-ranged attraction giving rise to a sharply peaked $g(r)$ and is accounted for qualitatively by the RPA. The height of the first peak does not vary rapidly with η_2^r and we find that freezing occurs when $S(k_m) \sim 1.04$ for $\eta_1=0.05$ and ~ 1.52 for $\eta_1=0.30$. These values of the peak height are *much* smaller than the peak height $S(k_m) \approx 2.85$ which, according to the Hansen-Verlet (one-phase) criterion [70], is supposed to signal the onset of freezing in simple fluids. Note that upon increasing η_1 the value of $S(k=0)$ is decreased and $S(k_m)$, and the heights of the subsequent maxima, is increased. These features simply

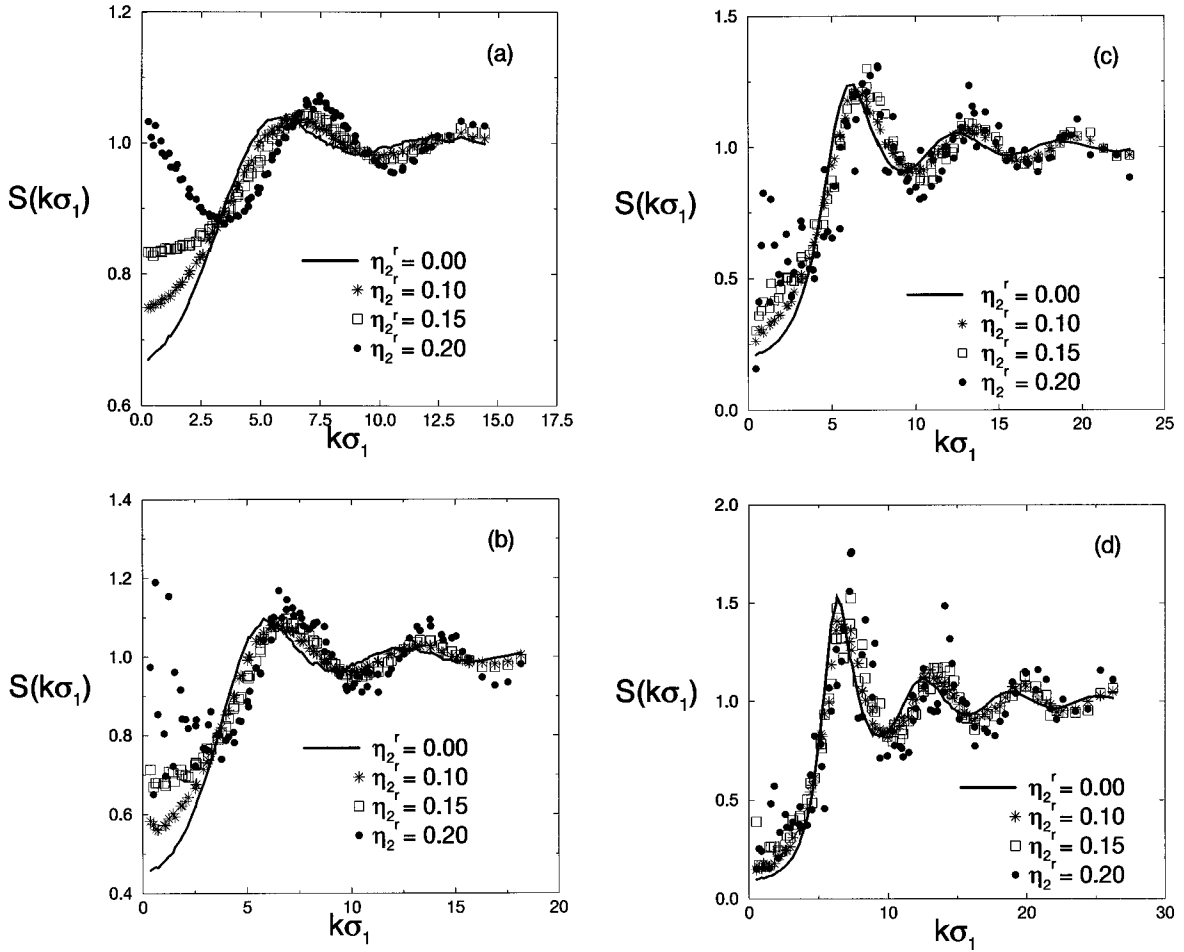


FIG. 10. The structure factor $S(k)$ for the effective one-component system, based on the depletion potential (33) with size ratio $q = 0.1$, small-sphere reservoir packing fractions $\eta_2^r = 0.00, 0.10, 0.15$, and 0.20 , and large-sphere packing fractions η_1 : (a) 0.05 , (b) 0.10 , (c) 0.20 , and (d) 0.30 . These are the same state points as in Fig. 9.

reflect the effect of increased packing of the large spheres in this effective one-component fluid.

In Fig. 11 we plot $g(r)$ for the less extreme size ratio $q = 0.2$ at several η_2^r for (a) $\eta_1 = 0.10$, (b) $\eta_1 = 0.20$, and (c) $\eta_1 = 0.30$. Upon increasing η_2^r at fixed η_1 we observe features that are similar to those for $q = 0.10$; namely, (i) the contact value of $g(r)$ increases, (ii) the minimum near $r = 1.15\sigma_1$ becomes more pronounced (note that the minimum is broader than for $q = 0.1$, reflecting the difference in the depletion potentials—see Fig. 1), and (iii) the peak at $r = 2\sigma_1$ becomes more pronounced. Once again there is no clear signature in $g(r)$ that phase separation has occurred. The structure factors for the same state points are shown in Fig. 12. The main features are similar to those for $q = 0.1$: $S(k=0)$ increases with increasing η_2^r for fixed η_1 and for states within the fluid-solid coexistence region the data become noisier. Upon increasing η_2^r , the position of the first maximum k_m again shifts to larger values. Finally we note that, as for $q = 0.1$, the values of $S(k_m)$ at the fluid-solid transition are much lower, for the three values of η_1 , than the value given by the Hansen-Verlet criterion [70]. Only when freezing occurs at high values of the packing fraction, $\eta_1 \geq 0.45$, should we expect this criterion to be valid. For the present system this would restrict its validity to the regime

$\eta_2^r \leq 0.15$ for $q = 0.2$ and to $\eta_2^r \leq 0.1$ for $q = 0.1$, where the freezing is (essentially) that of pure hard spheres. However, this is not known in advance.

VI. RESULTS OF DIRECT SIMULATIONS OF THE MIXTURE

In the previous section, we determined the phase behavior of a binary mixture of hard spheres using an effective one-component Hamiltonian based on pairwise additive depletion potentials. It is important to keep in mind that this Hamiltonian does not constitute an exact treatment of the binary system, since three- and higher-body interactions were neglected. One might expect the pairwise approximation to break down at sufficiently high densities (e.g., in the solid phase) or for less extreme size ratios (e.g., $q > 0.154$, where three nonoverlapping large spheres can overlap with a small one [61]), thereby casting doubt on the specific predictions (in particular those for the solid-solid transition). Moreover, the potential ϕ_{dep} used in the simulations is approximated by an empirical form that does not take into account the presence of longer-ranged oscillations [8]. To the best of our knowledge these approximations—and therefore the depletion potential picture as a whole—have never been tested

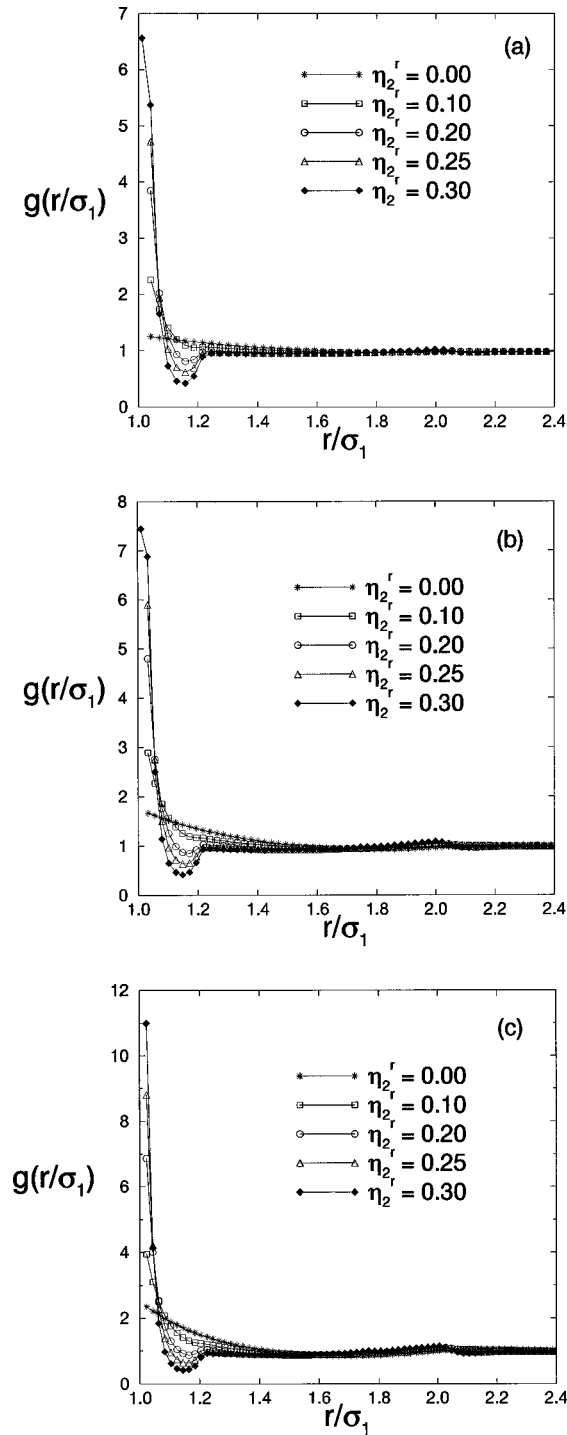


FIG. 11. The radial distribution function $g(r/\sigma_1)$ for the effective one-component system, based on the depletion potential (33) with size ratio $q=0.2$, small-sphere reservoir packing fractions $\eta_{2r}^r = 0.00, 0.10, 0.20, 0.25$ and 0.30 , and large-sphere packing fractions η_1 : (a) 0.10, (b) 0.20, and (c) 0.30. Note that fluid-solid coexistence occurs when $\eta_{2r}^r \approx 0.285$ for (a), $\eta_{2r}^r \approx 0.255$ for (b), and $\eta_{2r}^r \approx 0.23$ for (c).

directly by making a comparison with results of a full treatment of the true binary mixture. Given the richness of the predicted phase diagrams and the experimental and computational effort that is being put into the determination of the depletion potential, it is important to perform such test. It has been argued by many authors that direct simulations are not

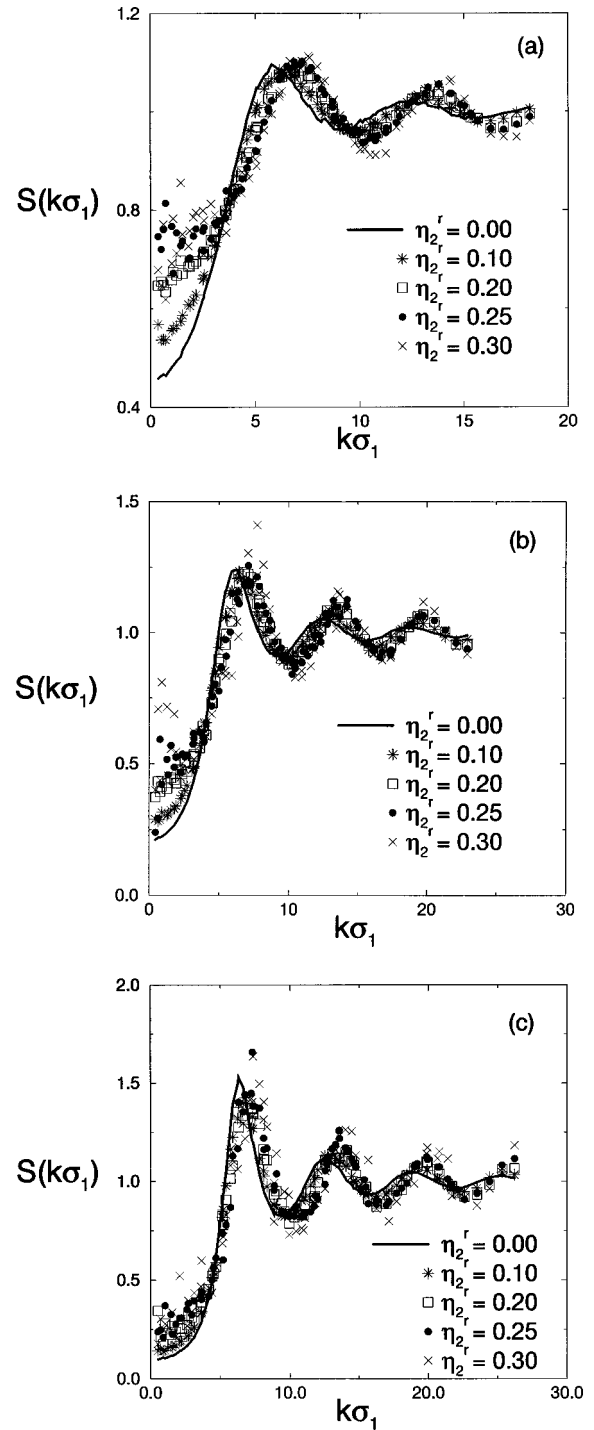


FIG. 12. The structure factor $S(k)$ for the effective one-component system, based on the depletion potential (33) with size ratio $q=0.2$, small-sphere reservoir packing fractions $\eta_{2r}^r = 0.00, 0.10, 0.20, 0.25$, and 0.30 , and large-sphere packing fractions η_1 : (a) 0.10, (b) 0.20, and (c) 0.30. These are the same state points as in Fig. 11.

feasible for highly asymmetric binary hard-sphere mixtures because of the ergodicity problems mentioned in the Introduction. However, the results in Fig. 4 show such interesting phase behavior at (surprisingly) low η_{2r}^r that we were motivated to perform direct simulations in this regime, using a scheme, to be discussed below, designed to deal with this regime, but not with the whole phase diagram. Our scheme

complements the direct simulations performed recently by Buhot and Krauth [68]. Their new algorithm is designed to deal with small-size ratios but it does not seem feasible [68] to implement the algorithm for most of the state points of interest here ($\eta_1 + \eta_2 > 0.25$).

The scheme we use to calculate the “exact” phase diagrams of binary hard-sphere mixtures by direct simulation employs the identity

$$\beta F(N_1, V, z_2) = \beta F(N_1, V, z_2 = 0) + \int_0^{z_2} dz_2' \left(\frac{\partial \beta F(N_1, V, z_2')}{\partial z_2'} \right). \quad (39)$$

The system at $z_2 = 0$ is the pure system of large hard spheres. Hence the first term of the right hand side of Eq. (39) is given accurately by the Carnahan-Starling [73] free energy in the fluid phase and by that of Hall [74] in the solid phase, as discussed already. The integrand in the second term can be rewritten using Eqs. (4) and (5) as

$$\left(\frac{\partial \beta F(N_1, V, z_2)}{\partial z_2} \right) = - \frac{\langle N_2 \rangle_{z_2}}{z_2}, \quad (40)$$

where $\langle N_2 \rangle_{z_2}$ denotes the average number of small particles in the (N_1, V, z_2) ensemble. This quantity can be measured directly in a grand-canonical simulation of the “adsorption” of small spheres from a reservoir at fugacity z_2 onto a system of N_1 large spheres in a volume V . Note that this scheme is almost identical to the widely known λ -integration scheme presented in Eq. (38) and in Ref. [81].

Before discussing the results of the direct simulations, we wish to make two remarks. First, the scheme proposed in Eqs. (39) and (40) is merely a bulk analog of using the Gibbs adsorption equation to determine the surface tension, where $\langle N_2 \rangle_{z_2}$ plays the role of the adsorption, F that of the surface tension, and N_1 , V , and q characterize the “substrate.” Second, it is important to realize that $\langle N_2 \rangle_{z_2}$ is *not* identical to the unweighted average adsorption from the reservoir onto a system of *static* large hard spheres, since not all configurations of large spheres carry the same statistical weight. In fact, this weight is proportional to $\exp[-\beta H^{\text{eff}}]$, a quantity that is not known exactly as it involves empirical pair potentials and unknown higher-order interactions, as we have seen above. Consequently, the grand-canonical simulations that measure $\langle N_2 \rangle_{z_2}$ must be combined with a *simultaneous* canonical average over the large-sphere configurations. This requirement still leads to ergodicity problems at high η_2^r , although the upper bound, which depends on N_1 , V , and q , is sufficiently high even for q as small as 0.05 to permit us to study interesting regimes.

We now return to the calculation of F from Eqs. (39) and (40). In Fig. 13, we plot $\eta_2 = \pi \sigma_2^3 \langle N_2 \rangle_{z_2} / 6V$, as a function of η_2^r , as measured in a simulation with $N_1 = 32$ for several η_1 . Results are shown for $q = 0.1$ and $q = 0.05$. Here we converted z_2 into η_2^r using the Carnahan-Starling expression $z_2 \sigma_2^3 = (6 \eta_2^r / \pi) \exp[(8 \eta_2^r - 9 \eta_2^{r2} + 3 \eta_2^{r3})(1 - \eta_2^r)^{-3}]$, which is essentially exact in the regime of interest. Although $N_1 = 32$ may seem too small a number of large spheres to per-

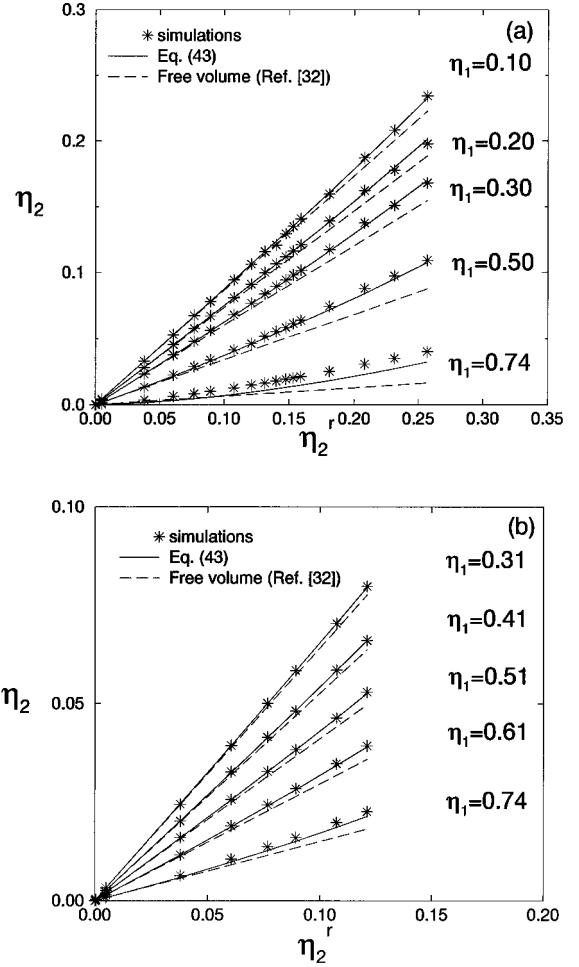


FIG. 13. The small-sphere packing fraction η_2 of a hard-sphere mixture with size ratio (a) $q = 0.10$ and (b) $q = 0.05$ versus that of the reservoir η_2^r for several large-sphere packing fractions η_1 . The asterisks denote simulation data while the solid lines denote the results obtained from the expressions of Henderson for the one-body term [66]. Dashed lines denote the results of the free volume approach [32].

form reliable simulations, one should recognize that (i) the pure large-sphere free energy (at $z_2 = 0$) is taken from accurate independent sources [73,74] and (ii) the maximum value of $\langle N_2 \rangle_{z_2}$ is about 5×10^4 due to the small-size ratios. We also plot η_2 as predicted by the scaled particle expressions for the zero- and one-body terms and the predictions of the free volume approach of Ref. [32]; these comparisons will be discussed in more detail in Sec. VII.

Using the simulation data for η_2 as a function of η_2^r or z_2 , we calculate $F(N_1, V, z_2)$ from Eq. (39) by numerical integration. Once F is known we employ common tangent constructions at fixed z_2 to obtain the phase boundaries shown by the symbols in Fig. 14. The main observation is the strikingly good overall agreement with the effective one-component results for the three values of the size ratio, $q = 0.2, 0.1$, and 0.05 , that we consider. Such good agreement throughout the fluid-solid coexistence curve for $q = 0.2$ and at high η_1 for $q = 0.1$ and 0.05 is rather unexpected, as one might expect the depletion picture to break down in these regimes. The only significant difference is that the isostructural solid-solid transition for $q = 0.1$ at $\eta_2^r \sim 0.06$ turns out to

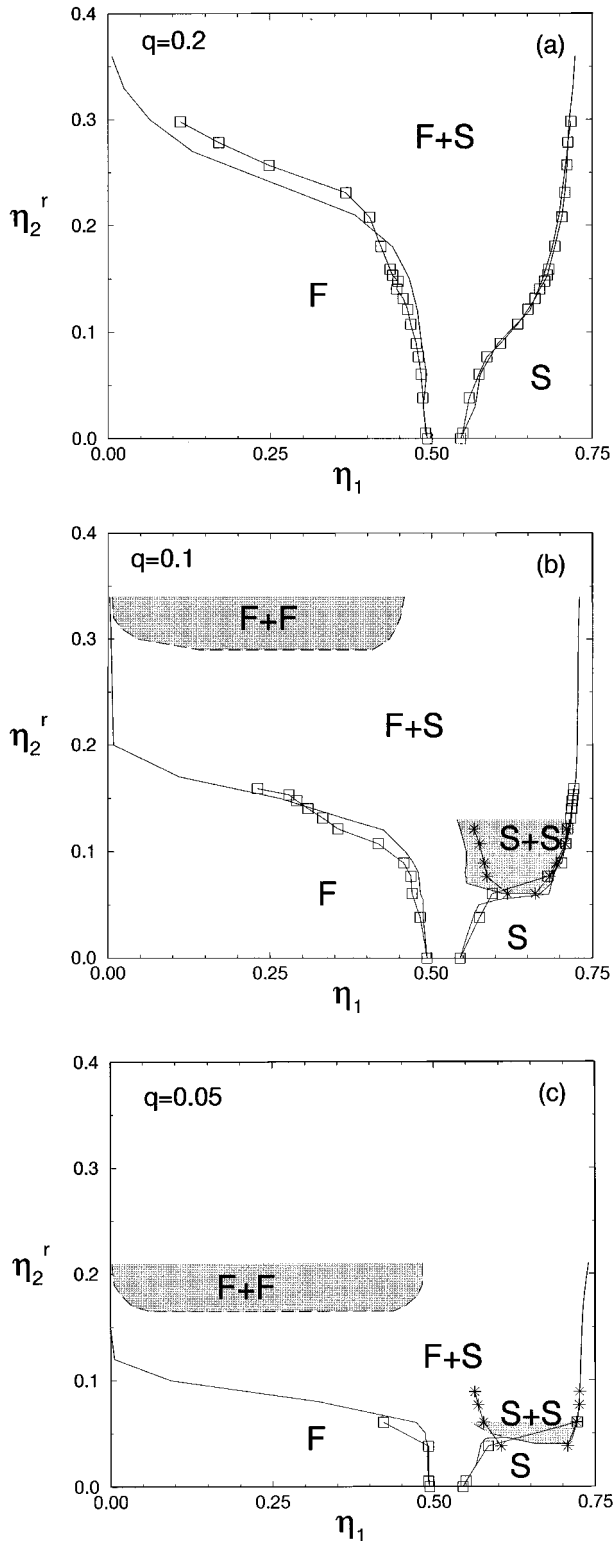


FIG. 14. Phase diagram of binary hard-sphere mixtures with size ratios (a) $q=0.2$, (b) $q=0.1$, and (c) $q=0.05$ as a function of the large-sphere packing fraction η_1 and the small-sphere reservoir packing fraction η_2^r . F and S denote the stable fluid and solid (fcc) phase. $F+S$, $F+F$, and $S+S$ denote, respectively, the stable fluid-solid, the metastable fluid-fluid, and the (meta)stable solid-solid coexistence regions. The solid and dashed lines are the effective one-component results; the squares and the asterisks (joined by lines to guide the eye) denote, respectively, the fluid-solid and the solid-solid transition obtained from direct simulations of the true binary mixture.

be stable with respect to fluid-solid coexistence, in contrast to the effective one-component prediction. The present results provide further evidence for a fluid-solid coexistence broadening with increasing η_2^r for all q , and do not support the narrowing predicted by some theoretical approaches [46,49]. Unfortunately, ergodicity problems prevented us from reaching the fluid-fluid demixing regime by direct simulation, so that this feature of the effective one-component results could not be tested. Nevertheless, the quantitative agreement at the accessible values of η_2^r does not give any indication that breakdown of the depletion potential picture will occur at higher η_2^r —at least not until the small spheres freeze.

As we computed the average number of small particles, $\langle N_2 \rangle_{z_2}$, in the (N_1, V, z_2) ensemble by direct simulation of the true binary mixture, we can convert our phase diagrams from the (η_1, η_2^r) plane to the (η_1, η_2) plane. In Fig. 15, we show the converted phase diagrams (open squares and asterisks) for $q=0.2, 0.1$, and 0.05 . Note that the tie lines are no longer horizontal.

In Fig. 16, we show snapshots of typical configurations of a binary hard-sphere mixture with a size ratio $q=0.1$ at small-sphere packing fractions $\eta_2^r=0.121$ and large-sphere packing fractions $\eta_1=0.30$ and $\eta_1=0.72$. These state points lie in single-phase regions but the densities are close to the coexisting fluid ($\eta_1=0.355$) and solid ($\eta_1=0.712$) densities at this value of η_2^r . In the solid phase, the large hard spheres form a face-centered-cubic lattice structure, while the small spheres are still disordered and fluidlike. Note that in both the fluid and solid phases η_2 is considerably smaller than η_2^r ; in the present case η_2 for the coexisting fluid is 0.069 while η_2 in the coexisting solid is 0.0174. These values are, of course, reflected in the pronounced (negative) slope of the tie lines in Fig. 15.

The coexisting densities obtained from direct simulations of the binary mixture are tabulated in Tables V, VI, and VII.

VII. DISCUSSION

A. Comparison with experiments and previous simulation studies

In order to compare our phase diagrams with experimental data and other simulation studies, we need to convert the reservoir packing fraction η_2^r of the small spheres to that in the binary mixture, η_2 . In the case of direct simulations, we computed the average number of small particles explicitly in the (N_1, V, z_2) ensemble and this allows us to convert the phase diagrams directly to the (η_1, η_2) plane. Figure 15 shows the converted phase diagrams for $q=0.2, 0.1$, and 0.05 . However, ergodicity problems prevented us from going to high η_2^r , and only a small part of the phase diagram could be studied directly by simulations of the true binary mixture. Using the effective Hamiltonian approach we could map out the phase diagram for higher η_2^r . In principle, the phase diagrams based on the effective Hamiltonian can be converted by employing the exact thermodynamic relation

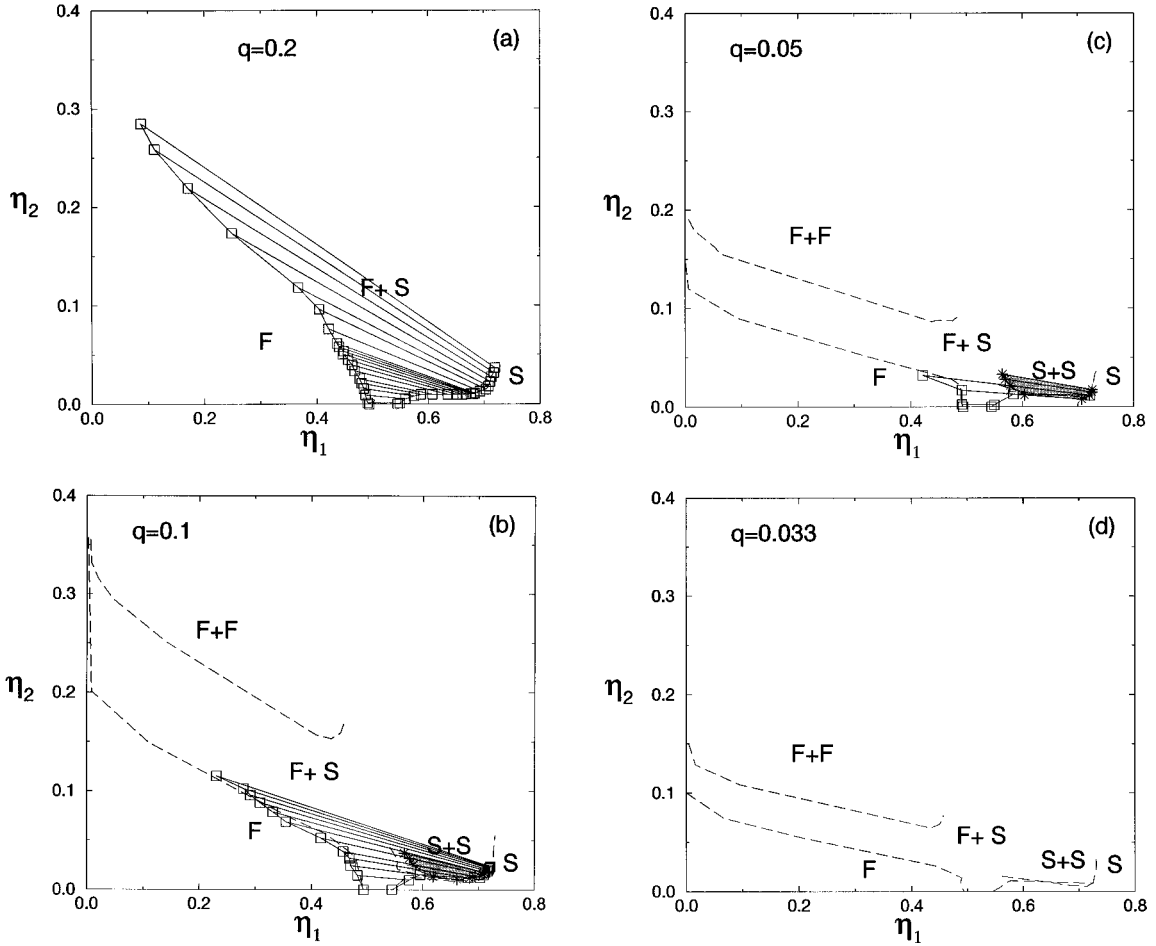


FIG. 15. Phase diagram of binary hard-sphere mixtures with size ratios (a) $q=0.2$, (b) $q=0.1$, (c) $q=0.05$, and (d) $q=0.033$ as a function of the large-sphere packing fraction η_1 and the small-sphere packing fraction η_2 . F and S denote the stable fluid and solid (fcc) phase. $F+S$, $F+F$, and $S+S$ denote, respectively, the stable fluid-solid, the metastable fluid-fluid and the (metastable) solid-solid coexistence regions. The squares and the asterisks (joined by lines to guide the eye) denote, respectively, the fluid-solid and the solid-solid phase boundaries obtained from direct simulations of the true binary mixture. The accompanying tie lines, which connect the coexisting densities (packing fractions), are also shown. In (b), (c), and (d) the dashed lines are the phase boundaries obtained from the effective Hamiltonian approach converted using Eq. (43). Note the differences in the vertical scales between the figures.

$$\langle N_2 \rangle_{z_2} = - \frac{\partial \beta F(N_1, V, \mu_2)}{\partial \beta \mu_2} = - \frac{\partial \beta (\Omega_0 + \Omega_1)}{\partial \ln z_2} - \left\langle \frac{\partial \beta \left(\sum_{n=2}^{N_1} \Omega_n \right)}{\partial \ln z_2} \right\rangle_{z_2}, \quad (41)$$

where we have used Eqs. (4), (13) and the notation $\langle \dots \rangle_{z_2}$ introduced in Sec. VI. In our calculation of the phase diagrams we ignored the zero- and one-body terms Ω_0 and Ω_1 , as these terms are irrelevant for the phase behavior and no direct information was obtained for $\langle N_2 \rangle_{z_2}$. However, the following scaled particle expressions can be employed for the quantities entering the zero- and one-body terms [66]:

$$\beta p_{\text{hs}}(z_2) = \frac{6}{\pi \sigma_2^3} \frac{\eta_2^r + (\eta_2^r)^2 + (\eta_2^r)^3}{(1 - \eta_2^r)^3}, \quad (42)$$

$$\beta \gamma_{\text{hs}}(z_2, R_1) = - \frac{9(\eta_2^r)^2}{2\pi\sigma_2^2} \frac{1 + \eta_2^r - 2\eta_2^r q}{(1 - \eta_2^r)^3},$$

$$\beta K(z_2) = \frac{-2\eta_2^r + 7(\eta_2^r)^2 - 11(\eta_2^r)^3}{2(1 - \eta_2^r)^3} - \ln(1 - \eta_2^r);$$

see Eqs. (19), (30), and (31). The conversion of z_2 into η_2^r can be made using the Carnahan-Starling expression $z_2 \sigma_2^3 = (6\eta_2^r/\pi) \exp[(8\eta_2^r - 9\eta_2^{r2} + 3\eta_2^{r3})(1 - \eta_2^r)^{-3}]$. By neglecting the two- and more-body interactions, the average number of particles of species 2 can then be approximated by

$$\langle N_2 \rangle_{z_2} \approx - \frac{\partial \beta (\Omega_0 + \Omega_1)}{\partial \ln z_2} = \frac{\partial \beta p_{\text{hs}}(z_2) [1 - \eta_1(1+q)^3] V}{\partial \ln z_2} - \frac{\partial [\beta \gamma_{\text{hs}}(z_2, R_1) \pi \sigma_1^2 N_1 + \beta K(z_2) N_1]}{\partial \ln z_2}. \quad (43)$$

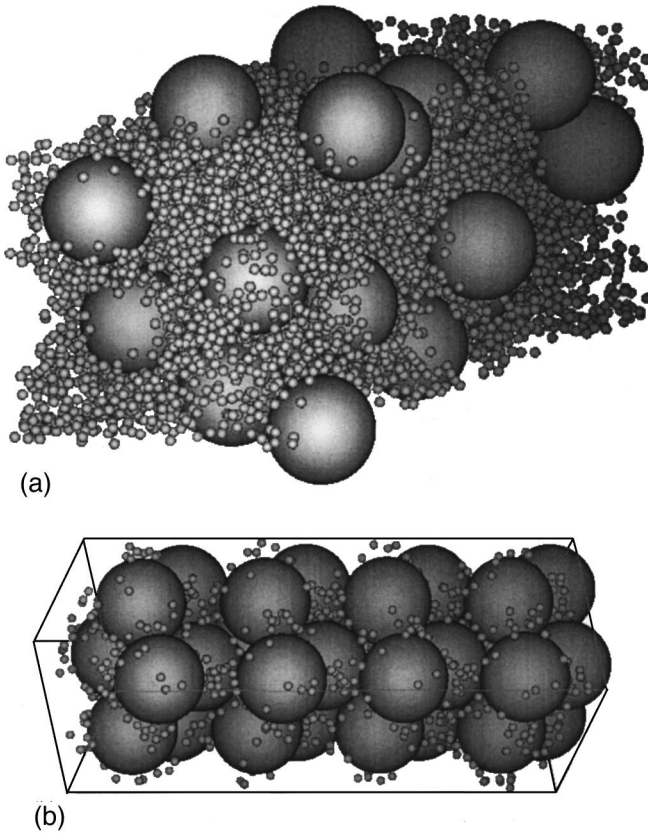


FIG. 16. Snapshots of typical configurations of a binary hard-sphere mixture with a size ratio $q=0.1$ at small-sphere reservoir packing fraction $\eta_2^r=0.121$ and large-sphere packing fraction (a) $\eta_1=0.30$, which corresponds to a stable fluid phase, and (b) $\eta_1=0.72$, which corresponds to a stable solid (fcc) phase.

We tested this approximate conversion against the data obtained from direct simulations of the true binary mixture. In Fig. 13, we plot η_2^r versus η_2 for size ratios $q=0.1$ and 0.05 for several large-sphere packing fractions η_1 . In general we found very good agreement with the expression (43) [82]. For comparison we also plot η_2 as predicted by the free volume approach of Ref. [32]; these results will be discussed in more detail in Sec. VII B. Using Eq. (43), we now convert our phase diagrams based on the effective Hamiltonian approach from the (η_1, η_2^r) plane to the (η_1, η_2) plane. These are also plotted, together with the conversions of the direct simulations, in Fig. 15. As expected on the basis of Figs. 13 and 14, the agreement between the two sets of results after the different conversions is good.

We now compare our $q=0.1$ phase diagram with the experimental data from [38] and [39]. In Fig. 17 we plot the phase diagram obtained from the effective Hamiltonian approach in the (η_1, η_2) plane, using the conversion based on Eq. (43), along with the experimental state points.

Imhof and Dhont performed experiments for charged silica spheres with diameters 365 nm and 39 nm (size ratio $q=0.1075$) dispersed in dimethylformamide [39]. The polydispersity of the large and small spheres is about 0.03 and 0.12, respectively. The following correlations are striking, and require further attention: (i) The crosses, denoting a (meta)stable fluid state, are, for $\eta_2 < 0.08$, close to our stable fluid phase boundary. At higher η_2 , there is substantial de-

TABLE V. The coexisting densities [expressed in terms of the packing fractions of large (η_1) and small (η_2) spheres] at the fluid-solid transition for a binary mixture of hard spheres with size ratio $q=0.2$ and varying packing fractions η_2^r of small spheres in the reservoir as obtained from direct simulations of the true binary mixture.

η_2^r	η_1 (fluid)	Fluid-solid		
		η_2 (fluid)	η_1 (solid)	η_2 (solid)
0.00	0.494	0.00	0.545	0.00
5.021×10^{-3}	0.491	0.0010	0.549	0.00064
3.796×10^{-2}	0.487	0.0089	0.559	0.00515
6.055×10^{-2}	0.484	0.015	0.574	0.00783
7.669×10^{-2}	0.480	0.021	0.587	0.00962
8.923×10^{-2}	0.476	0.026	0.608	0.00953
0.107	0.467	0.033	0.635	0.00950
0.121	0.463	0.039	0.650	0.00967
0.131	0.456	0.045	0.662	0.00970
0.140	0.446	0.050	0.669	0.00999
0.147	0.448	0.053	0.676	0.01007
0.153	0.439	0.058	0.681	0.01014
0.159	0.436	0.061	0.683	0.01074
0.181	0.421	0.076	0.693	0.01261
0.208	0.404	0.096	0.703	0.01476
0.231	0.367	0.118	0.708	0.01770
0.257	0.248	0.173	0.711	0.02228
0.279	0.171	0.219	0.713	0.02723
0.298	0.112	0.259	0.717	0.03155
0.318	0.087	0.285	0.719	0.03666

viation. A possible reason for this deviation might be the polydispersity of the small spheres, which we plan to study in future work. Another reason might be the slow equilibration or kinetics of the phase transition resulting from gelation, vitrification, or amorphization [83–85]. (ii) The open squares, denoting the experimental state points that exhibit fluid-solid coexistence, are well inside our fluid-solid coexistence region, and extend to high η_1 if there is no metastable fluid-fluid or solid-solid binodal. (iii) The triangles, representing the observed glassy states, are all close to or within the metastable fluid-fluid or solid-solid binodal which we calculated. A similar link between the formation of non-equilibrium phases and the presence of metastable phase coexistence has been observed in experiments on colloid-polymer mixtures, and has been explained by a simple model for the diffusion-limited kinetics of phase ordering [86]. It should be noted that crystallization was only observed in these experiments [39] in a limited region of the phase diagram (where $\eta_1 > \eta_2$). The authors of Ref. [39] also measured the long-time self-diffusion of the large hard spheres in the mixture, and found an enormous decrease in the diffusion constant when small spheres are added. It is therefore not surprising that the crystallization rates become extremely small (or zero) at sufficiently high packing fractions of the small spheres.

Dinsmore *et al.* reported experiments on charge-stabilized polystyrene microspheres, dispersed in water, with a small-sphere diameter of 69 nm and large-sphere diameters ranging from 137 to 825 nm [38]. In contrast with the experiments of

TABLE VI. The coexisting densities at the fluid-solid and solid-solid transitions for a binary mixture of hard spheres with size ratio $q=0.1$ and varying packing fractions η_2^r of small spheres in the reservoir as obtained from direct simulations of the true binary mixture.

Fluid-solid				
η_2^r	η_1 (fluid)	η_2 (fluid)	η_1 (solid)	η_2 (solid)
0.00	0.494	0.000	0.545	0.0000
3.796×10^{-2}	0.483	0.014	0.576	0.0099
6.055×10^{-2}	0.470	0.024	0.595	0.0151
7.669×10^{-2}	0.468	0.032	0.681	0.0121
8.923×10^{-2}	0.457	0.039	0.703	0.0126
0.107	0.417	0.052	0.709	0.0151
0.121	0.355	0.069	0.712	0.0174
0.131	0.331	0.079	0.717	0.0188
0.140	0.308	0.088	0.718	0.0204
0.147	0.291	0.096	0.719	0.0217
0.153	0.279	0.102	0.720	0.0226
0.159	0.230	0.115	0.721	0.0235
Solid-solid				
η_2^r	η_1 (solid 1)	η_2 (solid 1)	η_1 (solid 2)	η_2 (solid 2)
6.055×10^{-2}	0.619	0.0134	0.662	0.0105
7.669×10^{-2}	0.587	0.0206	0.684	0.0120
8.923×10^{-2}	0.583	0.0249	0.694	0.0134
0.107	0.575	0.0317	0.708	0.0154
0.121	0.567	0.0369	0.710	0.0176

Imhof and Dhont [39], these authors did not find any crystallization problems at high η_2 . In Fig. 17, we plot the experimental state points that exhibit a clear fluid-solid coexistence in the bulk for binary mixtures with $q=0.1136$ and 0.0833 . We find that all the state points for $q=0.1136$ lie well inside, while the state points for $q=0.0833$ lie slightly below the fluid-solid binodal calculated for $q=0.1$. Thus, these experimental results are consistent with what we would expect from the trend in Fig. 15.

In Ref. [53], it is shown that for $q=0.1$ the RY and Ballone-Pastore-Galli-Gazzillo (BPGG) integral equation theories give a spinodal instability in the fluid phase, while the PY equation always predicts complete miscibility of the two species. For comparison we plot the RY and the BPGG spinodals in Fig. 17. We find that the BPGG spinodal lies well inside our fluid-fluid coexistence region, while the RY spinodal lies below the fluid-solid binodal. We also mention that the state point ‘‘A’’ ($\eta_1=0.244$, $\eta_2=0.072$) studied in

TABLE VII. The coexisting densities at the fluid-solid and solid-solid transitions for a binary mixture of hard spheres with size ratio $q=0.05$ and varying packing fractions η_2^r of small spheres in the reservoir as obtained from direct simulations of the true binary mixture.

Fluid-solid				
η_2^r	η_1 (fluid)	η_2 (fluid)	η_1 (solid)	η_2 (solid)
0.00	0.4938	0.0000	0.545	0.0000
5.021×10^{-3}	0.4916	0.0022	0.550	0.0018
3.796×10^{-2}	0.4915	0.0165	0.584	0.0127
6.055×10^{-2}	0.4219	0.0318	0.722	0.0116
Solid-solid				
η_2^r	η_1 (solid 1)	η_2 (solid 1)	η_1 (solid 2)	η_2 (solid 2)
3.796×10^{-2}	0.6042	0.0119	0.7073	0.0075
6.055×10^{-2}	0.5776	0.0211	0.7212	0.0116
7.669×10^{-2}	0.5691	0.0277	0.7255	0.0146
8.923×10^{-2}	0.5640	0.0329	0.7261	0.0172

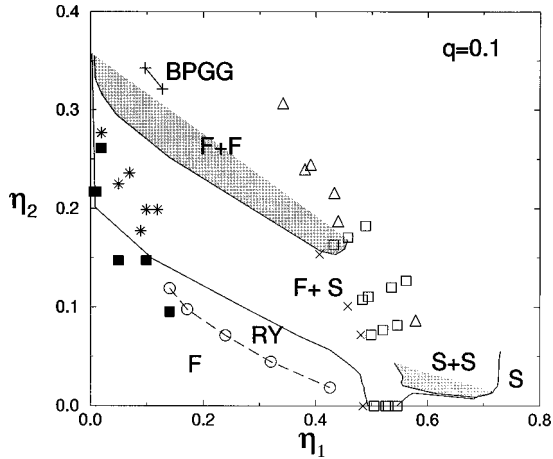


FIG. 17. Phase diagram of binary hard-sphere mixtures with a size ratio $q=0.1$ as a function of the large-sphere packing fraction η_1 and the small-sphere packing fraction η_2 . F and S denote the stable fluid and solid (fcc) phases. $F+F$ and $S+S$ denote, respectively, the stable fluid-fluid and the solid-solid coexistence regions. The solid lines denote, respectively, the fluid-fluid and the solid-fluid phase boundaries obtained from simulations based on the effective Hamiltonian approach and the conversion (43). The open triangles, crosses, and open squares are experimental state points taken from Ref. [39] where $q=0.1075$, representing glassy states, (meta)stable fluid phases, and fluid-solid demixing, respectively. The solid squares and asterisks denote the experimental state points taken from Ref. [38], representing fluid-solid demixing for a binary colloidal hard-sphere mixture with size ratio $q=0.0833$ and $q=0.1136$, respectively. The plusses and the open circles joined by a dashed line denote the theoretical BPGG and RY spinodal, respectively, taken from Ref. [53].

the simulations of Ref. [53] lies outside our fluid-solid coexistence region. For this state point good agreement is found between the pair distribution function of the larger species obtained from the BPGG integral equations, from simulations of the true binary mixture, and from simulations using the effective depletion potential [53]. On the other hand, the state point 'C' ($\eta_1=0.1$, $\eta_2=0.32$) lies well inside our metastable fluid-fluid binodal, which might explain the observed two-stage demixing dynamics. It is tempting to argue that the rapid clustering found at the first stage reflects the fluid-fluid binodal, while the subsequent slow relaxation of clusters signals the crystallization process.

We note finally that simulations of the full two-component system have been carried out recently for several values of q for the single state point $\eta_1=\eta_2=0.1215$ [68]. These authors computed the radial distribution function of the large spheres $g_{11}(r)$ in the mixture and in a pure system of large hard spheres. By comparing the integrated $g_{11}(r)$ in the mixture with that of the pure system, the authors inferred no, weak, and strong tendencies to demix for $q=0.1, 0.05$, and 0.033 , respectively. These inferences are consistent with the phase boundaries we calculate from the effective Hamiltonian: from Fig. 15 we see that the state point lies below the fluid-solid binodal for $q=0.1$, while for $q=0.033$ it lies inside the metastable fluid-fluid region. At $q=0.05$ the state point would be in the fluid-solid region, and so we identify the observed clustering as crystallization rather than the fluid-fluid demixing which was implied in [68].

B. Connection with free volume theory and colloid-polymer mixtures

There is a close connection between the hard-sphere mixtures studied in this paper and mixtures of colloidal hard spheres (with diameter σ_1) and nonadsorbing polymers (with radius of gyration R_g and diameter $\sigma_2=2R_g$). Such colloid-polymer mixtures resemble binary hard-sphere mixtures in the sense that the colloid-colloid and colloid-polymer interaction is hard-sphere like, with contact distances $\sigma_{11}=\sigma_1$ and $\sigma_{12}=(\sigma_1+\sigma_2)/2$, respectively. An important difference between such systems and additive binary mixtures of hard spheres is the interpenetrable character of the polymer-polymer interaction, which in the simplest (ideal) case is described by $\sigma_{22}=0$. This simple model for colloid-polymer mixtures is nonadditive, in contrast to the additive hard-sphere mixture studied in this paper. In Ref. [87], the thermodynamic potential of N_1 colloidal hard spheres in a volume V in contact with a reservoir of ideal polymers at fugacity z_2 is written as

$$F(N_1, V, z_2) = F(N_1, V, z_2=0) - \Pi_2' \langle V_{\text{free}} \rangle_{z_2=0}, \quad (44)$$

where Π_2' is the osmotic pressure of the polymer reservoir, and where $\langle V_{\text{free}} \rangle_{z_2=0}$ is the statistically averaged free volume (or nonexcluded volume) of a test polymer in the system of N_1 colloids at polymer fugacity $z_2=0$. Using scaled-particle (or Percus-Yevick) expressions, the so-called free volume approach represented by Eq. (44) predicts a fluid-fluid demixing transition for $q=\sigma_2/\sigma_1 \geq 0.35$ [87]. The mechanism behind this phase separation is the depletion effect, which results in the Asakura-Oosawa effective attraction between the colloidal particles arising from the presence of polymers [30,31]. One should realize, however, that the depletion effect is enhanced significantly by the nonadditivity of the interactions, which allows the number density of polymers, and thereby the strength of the depletion interaction, to be much larger than in additive mixtures [88].

Expression (44) was also used by Lekkerkerker and Stroobants to study additive binary hard-sphere systems [32]. In order to make a connection with their work, we rederive Eq. (44), starting from the exact results (39) and (40). This rederivation identifies clearly the approximations involved in Eq. (44). The first approximation involves the low- z_2 Taylor expansion of the second term in the right hand side of Eq. (39),

$$\int_0^{z_2} dz_2' \left(\frac{\partial \beta F(N_1, V, z_2')}{\partial z_2'} \right) = z_2 \left(\frac{\partial \beta F(N_1, V, z_2')}{\partial z_2'} \right) \Bigg|_{z_2'=0} + O(z_2^2). \quad (45)$$

The first, $O(z_2)$, term in Eq. (45) can be rewritten with Eqs. (4) and (9) as

$$\begin{aligned}
& z_2 \left(\frac{\partial \beta F(N_1, V, z_2')}{\partial z_2'} \right) \Bigg|_{z_2'=0} \\
&= -z_2 \frac{\text{Tr}_1 \left\{ \exp[-\beta H_{11}] \int_V d\mathbf{r}_1 \prod_{i=1}^{N_1} (1 + f_{i1}) \right\}}{\text{Tr}_1 \exp[-\beta H_{11}]} \\
&= -z_2 \langle V_{\text{free}} \rangle_{z_2'=0}, \tag{46}
\end{aligned}$$

which defines formally the free volume $\langle V_{\text{free}} \rangle_{z_2'=0}$ introduced already. It is easily seen from Eqs. (39), (40), (45), and (46) that

$$\beta F(N_1, V, z_2) = \beta F(N_1, V, z_2=0) - z_2 \langle V_{\text{free}} \rangle_{z_2'=0} + O(z_2^2), \tag{47}$$

which reduces to Eq. (44) if the $O(z_2^2)$ terms are neglected and $\beta \Pi_2^r$ is replaced by z_2 , its low-density limit. However, the free volume approach of Ref. [32] employs the Percus-Yevick result for $\beta \Pi_2^r$ [$\beta \Pi_2^r = \beta p_{\text{hs}}$; see Eq. (43)], which contains terms to all order in z_2 , while other $O(z_2^2)$ terms, arising from the integration, are not taken into account. In other words, the free volume approach of Ref. [32] involves nonsystematic $O(z_2^2)$ and higher-order terms. Furthermore, when we calculate the phase diagram that results from Eq. (44) but with $\beta \Pi_2^r$ replaced by z_2 , we find a much worse agreement with our simulation results for $q=0.1$ and 0.2 than when the Percus-Yevick result is used for $\beta \Pi_2^r$. Apparently, the nonsystematic procedure of replacing z_2 by $\beta \Pi_2^r$ in Eq. (47) gives rise to a better representation of the spinodal. This can be motivated, perhaps, by considering a further re-derivation of Eq. (44) starting from the exact expressions (39) and (40). We first introduce the quantity $\alpha(z_2, \eta_1) \equiv \eta_2(z_2, \eta_1) / \eta_2^r(z_2)$, i.e., the ratio of the density of small spheres in the mixture to that in the reservoir, for given fugacity z_2 and packing fraction η_1 of the large spheres. It is a trivial exercise to prove that $\langle N_2 \rangle / z_2 = V \alpha(z_2, \eta_1) \partial \beta \Pi_2^r / \partial z_2$, which upon inserting into Eqs. (39) and (40) and performing the integral by parts yields the exact result

$$\begin{aligned}
F(N_1, V, z_2) &= F(N_1, V, z_2=0) - \Pi_2^r(z_2) \alpha(z_2, \eta_1) V \\
&+ V \int_0^{z_2} dz_2' \Pi_2^r(z_2') \left(\frac{\partial \alpha(z_2', \eta_1)}{\partial z_2'} \right). \tag{48}
\end{aligned}$$

If one now approximates $\alpha(z_2, \eta_1)$ by its low- z_2 value $\alpha(z_2=0, \eta_1)$ —which can be interpreted as the free volume fraction of a small test sphere in a system of large spheres at packing fraction η_1 —it is easily seen that the last term in Eq. (48) vanishes, while the remaining expression is *identical* to Eq. (44). However, when the full, but unknown, expression for $\alpha(z_2, \eta_1)$ is used, the integral in Eq. (48) is expected to give at least $O(z_2^2)$ contributions, which, *a priori*, could be as important as $O(z_2^2)$ contributions from the term $\Pi_2^r \alpha V$ in Eq. (48). Thus, we conclude again that the free volume approach of Ref. [32] contains nonsystematic $O(z_2^2)$ contributions to the free energy.

The accuracy of the linear low- z_2 approximation $\eta_2 = \alpha(z_2=0, \eta_1) \eta_2^r$ —with the scaled particle expressions for $\alpha(z_2=0, \eta_1)$ —as employed in the free volume approach of Ref. [32], can be tested by comparison with the simulation results for η_2 as a function of z_2 and η_1 . The dashed line in Fig. 13 represents this linear relation while the symbols denote the simulation results and the solid curves those from approximation (43). Agreement with results of direct simulations is poorer than for the approximation (43) and becomes, as expected, worse with increasing η_2^r , for every value of η_1 . Moreover, the differences between simulation and theory begin at lower η_2^r when η_1 is higher [82]. The main difference between the linear low- z_2 approximation of the free volume approach and approximation (43) is the presence of the second term on the right hand side of Eq. (43), which can be interpreted as the adsorption of small spheres onto the surface of the large spheres [89].

It is important to note that neglecting the $O(z_2^2)$ terms in Eq. (45) actually involves two approximations: (i) The interaction between the smaller species (g bonds) is neglected, which is justified for ideal polymers but *not* for hard spheres. This assumption implies that the two-body term ω_2 is the Asakura-Oosawa pair potential, which is often used to describe colloid-polymer mixtures [30,31]. However, it does not imply that three- and more-body interactions between the colloidal particles are neglected. The free volume itself includes the effects of these higher-order interactions. (ii) An equal statistical weight is assigned to all (nonoverlapping) large-sphere configurations, whereas the weight should be proportional to $\exp[-\beta H^{\text{eff}}]$; i.e., the weight should involve the effective interactions.

We remark that when $\eta_2^r \rightarrow 0$ the depletion potential (33) reduces to the Asakura-Oosawa pair potential calculated in the Derjaguin approximation, appropriate to small values of q . Since the interesting (η_1, η_2^r) regime for $q \rightarrow 0$ corresponds to very small η_2^r , our phase diagrams for very asymmetric additive hard-sphere mixtures should resemble those of very asymmetric nonadditive colloid-polymer mixtures. Indeed, the fluid-solid transition for nonadditive colloid-polymer mixtures with $q=0.1$ and 0.2 , calculated by Gast *et al.* within a second-order perturbation theory treatment of the Asakura-Oosawa pair potential—see Fig. 6 of [61]—resembles the phase diagrams of our Fig. 4. These authors also reported a fluid-fluid transition for $q=0.2$, but not for $q=0.1$. A solid-solid transition was not reported in Ref. [61].

C. Conclusions

In summary, we have investigated the phase behavior and structure of highly asymmetric binary hard-sphere mixtures. An expression for the effective Hamiltonian of the large spheres was derived by formally integrating out the degrees of freedom of the small spheres. We showed that this Hamiltonian consists of zero-body, one-body, two-body, and higher-body terms. The two-body term is the usual depletion potential, and the zero-body and one-body terms play no role in determining the phase behavior. Using an accurate approximation for the effective pair potential and neglecting higher-body terms, we determined, by standard one-component simulation methods, the phase behavior of binary hard-sphere mixtures, finding a broad fluid-solid coexistence

for mixtures with a size ratio $q \leq 1$, a *metastable* fluid-fluid transition for $q \leq 0.10$, and a stable solid-solid coexistence for $q \leq 0.05$. The structure of the effective one-component system was studied by computing the radial distribution function and the structure factor. There is no sharp change in these functions as the fluid-solid binodal is crossed. However, for states in the two-phase region $S(k)$ exhibits an increase as $k \rightarrow 0$ and becomes very noisy, features that might be identified with clustering of the large spheres. In addition we find that the Hansen-Verlet freezing criterion does not provide an accurate estimate for the onset of freezing over a large fraction of the fluid-solid phase boundary.

Since these effective one-component calculations predicted interesting phase behavior at such low packing fractions of the small spheres, we were motivated to show that direct simulations of the true binary mixture *are* feasible in these regimes. We performed such direct simulations for $q = 0.05, 0.1, \text{ and } 0.2$, and for the range of packing fractions accessible to direct simulations, we found remarkably good agreement with the phase diagrams resulting from the effective one-component simulations. Bearing in mind the sensitivity to details found in earlier attempts to determine the phase diagrams of highly asymmetric binary hard-sphere mixtures, the quantitative consistency between the results of these completely independent calculations lends strong support to the reliability of our phase diagrams — at least for those regimes where direct simulations can be performed. We conclude that the use of the effective pairwise depletion description is well justified for the size ratios $q = 0.05, 0.1, \text{ and } 0.2$. It follows that this description should remain reliable for more asymmetric cases, i.e., $q \leq 0.05$. (Indeed one might argue that this description should become more accurate, since higher-body terms should be less important and the detailed form of the depletion potential is better established [54] for very-small-size ratios.) Thus, we are rather confident about our predictions for $q = 0.033$, for example. In particular, we predict that the fluid-fluid transition will remain metastable with respect to the fluid-solid transition as $q \rightarrow 0$.

We close with some final, hopefully provocative, remarks: (i) The fluid-solid coexistence regions in Fig. 15 (even for relatively mild asymmetry, say, $q = 0.2$) are extremely broad. This means that caution must be exercised when studying the properties of asymmetric binary hard-sphere *fluids*, so as not to enter the two-phase region. We suspect that several published theoretical and, perhaps, simulation studies correspond to a bulk two-phase region. The repercussions should be investigated further. (ii) The pairwise depletion potential description appears to account satisfactorily for the phase equilibria for surprisingly *large* values of q . It is not clear why this should be the case and further investigations are required to assess the regime of validity of the pairwise approximation. (iii) Although the effective Hamiltonian does appear to provide an accurate account of the phase behavior of asymmetric binary hard-sphere mixtures, it has not been ascertained how accurate this is for describing the structure, i.e., for the radial distribution function of the large spheres, $g_{11}(r)$. For the true binary mixture it is known that all three radial distribution functions $g_{11}(r)$, $g_{22}(r)$, and $g_{12}(r)$ exhibit the same characteristic asymptotic ($r \rightarrow \infty$) decay. The exponential decay length and

the period of the oscillations are the same for all three distribution functions and depend on the packing fractions and sizes of both species [90]. It is difficult to see how $g(r)$ computed from the effective depletion potential, which is evaluated at infinite dilution of the large spheres, can incorporate *all* the features of the true $g_{11}(r)$. This topic also warrants further investigation.

ACKNOWLEDGMENTS

This work was made possible by financial support from the EC by Grant Nos. ERBFMBICT972446 and ERBFMBICT971869 of the TMR program, and by the EPSRC under Grant No. GR/L89013. We thank D. Frenkel and H.N.W. Lekkerkerker for stimulating discussions.

APPENDIX: COMMON TANGENT CONSTRUCTION IN THE (N_1, μ_2, V, T) ENSEMBLE

The Helmholtz free energy of a binary (hard-core) mixture with particle numbers N_1 and N_2 in a volume V is given by $F_c(N_1, N_2, V)$, where we omitted the explicit temperature dependence. It proves convenient, however, to consider the system in the (N_1, μ_2, V, T) ensemble, in which the chemical potential μ_2 of species 2 is fixed instead of the corresponding particle number N_2 . The associated thermodynamic potential is denoted $F(N_1, \mu_2, V, T)$, and is related to F_c by the Legendre transform

$$F(N_1, \mu_2, V) = F_c(N_1, N_2, V) - \mu_2 N_2. \quad (\text{A1})$$

Here we describe how phase equilibria can be determined from knowledge of F . Since F is extensive for macroscopically large N_1 and V , we can write

$$F(N_1, \mu_2, V) = \frac{6V}{\pi\sigma_1^3} f(\mu_2, \eta_1), \quad (\text{A2})$$

where $\eta_1 = \pi\sigma_1^3 N_1 / 6V$ is the packing fraction of species 1 and $f(\mu_2, \eta_1)$ is a dimensionless free energy density of the binary mixture at a chemical potential μ_2 . The pressure P of the binary system is given by

$$\begin{aligned} P(\mu_2, v_1) &= - \left(\frac{\partial F_c(N_1, N_2, V)}{\partial V} \right)_{N_1, N_2} \\ &= - \left(\frac{\partial F(N_1, \mu_2, V)}{\partial V} \right)_{N_1, \mu_2} \\ &= \frac{-6}{\pi\sigma_1^3} \left[f(\mu_2, \eta_1) - \eta_1 \left(\frac{\partial f(\mu_2, \eta_1)}{\partial \eta_1} \right)_{\mu_2} \right], \end{aligned} \quad (\text{A3})$$

and the chemical potential μ_1 of species 1 is given by

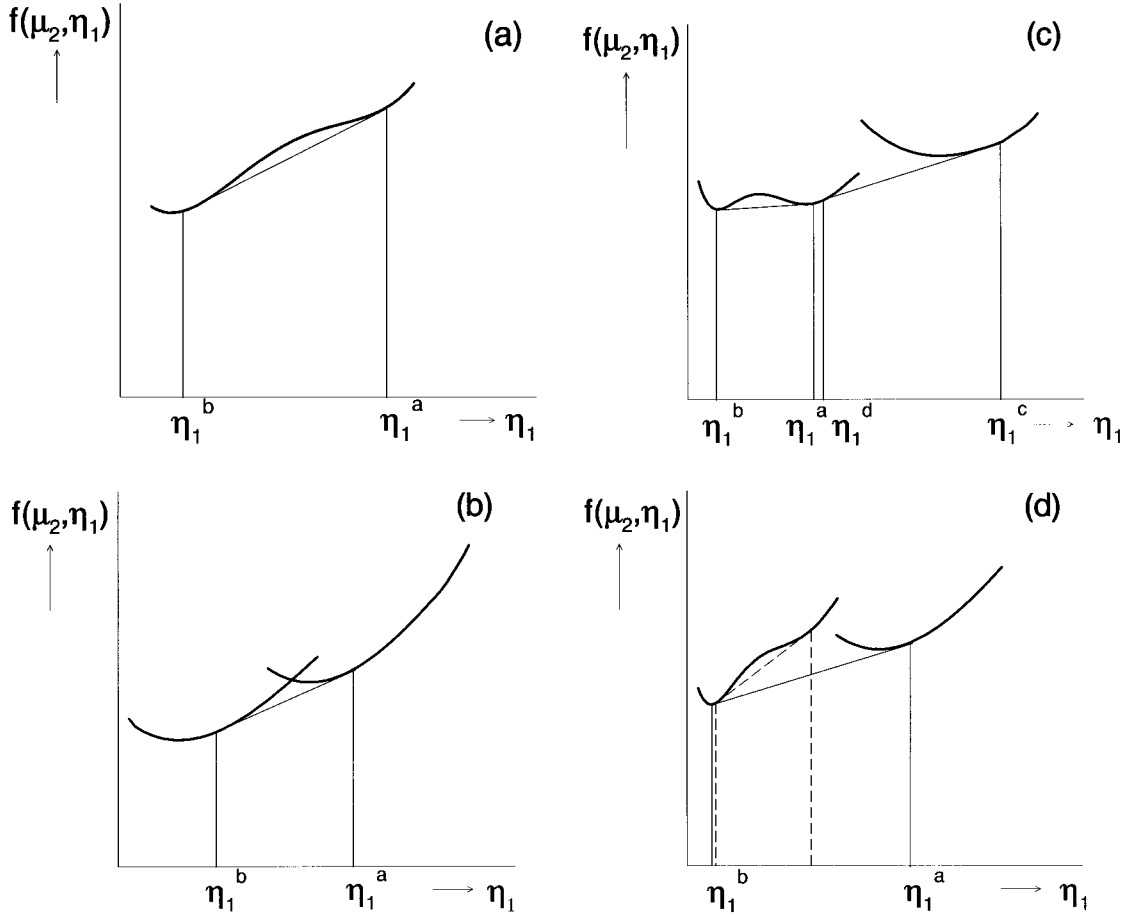


FIG. 18. The dimensionless free energy density $f(\mu_2, \eta_1)$ versus the packing fraction η_1 . Schematic illustration of the common tangent construction to determine the phase coexistence in binary mixtures. (a) Symmetry conserved coexistence (fluid-fluid or isostructural solid-solid coexistence), (b) symmetry broken coexistence (fluid-solid coexistence), (c) a stable symmetry conserved and a stable symmetry broken coexistence, and (d) a metastable symmetry conserved coexistence (dashed line) and a stable symmetry broken coexistence (thin solid line).

$$\begin{aligned} \mu_1(\mu_2, v_1) &= \left(\frac{\partial F_c(N_1, N_2, V)}{\partial N_1} \right)_{N_2, V} = \left(\frac{\partial F(N_1, \mu_2, V)}{\partial N_1} \right)_{\mu_2, V} \\ &= \left(\frac{\partial f(\mu_2, \eta_1)}{\partial \eta_1} \right)_{\mu_2}, \end{aligned} \quad (\text{A4})$$

where, in the second steps, we used $\mu_2 = (\partial F_c / \partial N_2)_{N_1, V, T}$. The pressure and the chemical potentials of both species are important quantities in the determination of phase boundaries at first-order transitions, where two phases with different packing fractions of species 1 (and 2) coexist. The conditions for the coexistence of two phases, say, a and b , with packing fractions η_1^a and η_1^b and chemical potential μ_2 (or fugacity z_2), are mechanical equilibrium $P^a(\mu_2, \eta_1^a) = P^b(\mu_2, \eta_1^b)$ and chemical equilibrium $\mu_1^a(\mu_2, \eta_1^a) = \mu_1^b(\mu_2, \eta_1^b)$. Invoking these two conditions with Eqs. (A3) and (A4) yields

$$\left. \frac{\partial f}{\partial \eta_1} \right|_{\eta_1^a} = \left. \frac{\partial f}{\partial \eta_1} \right|_{\eta_1^b} = \frac{f(\mu_2, \eta_1^a) - f(\mu_2, \eta_1^b)}{\eta_1^a - \eta_1^b}. \quad (\text{A5})$$

Geometrically this representation corresponds to the so-called common tangent construction for determining η_1^a and η_1^b . This is illustrated in Fig. 18, where we plot schematically $f(\mu_2, \eta_1)$ for a symmetry-conserving transition (e.g., fluid-fluid or isostructural solid-solid transition) and for a symmetry-breaking transition (e.g., fluid-solid transition). The physical interpretation of the common tangent construction, denoted by the thin solid lines in Fig. 18, is the usual one; i.e., the system in the regime $\eta_1^b < \eta_1 < \eta_1^a$ can lower its free energy by forming a linear combination of phases a and b .

It is also possible that two or more spinodal instabilities of the free energy curve are present. This is illustrated in Figs. 18(c) and 18(d). In Fig. 18(c), we illustrate the existence of a stable symmetry-conserving transition and a stable symmetry-breaking transition. In Fig. 18(d), we see once again the existence of a symmetry-conserving transition and a symmetry-breaking transition, but here the former is metastable with respect to the latter. Finally it is straightforward to show that adding terms to F which are linear in η_1 , whose coefficients are functions of z_2 , does not affect the values of the packing fractions at coexistence. One can make the common tangent construction with or without these terms.

- [1] W. W. Wood and J. D. Jacobson, *J. Chem. Phys.* **27**, 1207 (1957).
- [2] B. J. Alder and T. E. Wainwright, *J. Chem. Phys.* **27**, 1208 (1957).
- [3] T. Biben and J. P. Hansen, *Phys. Rev. Lett.* **66**, 2215 (1991); *J. Phys.: Condens. Matter* **3**, F65 (1991).
- [4] J. L. Lebowitz and J. S. Rowlinson, *J. Chem. Phys.* **41**, 133 (1964).
- [5] Y. Martinez-Raton and J. A. Cuesta, *Phys. Rev. E* **58**, R4080 (1998); J. A. Cuesta and Y. Martinez-Raton, *J. Chem. Phys.* **107**, 6379 (1997); *Phys. Rev. Lett.* **78**, 3681 (1997); J. A. Cuesta, *ibid.* **76**, 3742 (1996); M. Dijkstra, D. Frenkel, and J. P. Hansen, *J. Chem. Phys.* **101**, 3179 (1994); M. Dijkstra and D. Frenkel, *Phys. Rev. Lett.* **72**, 298 (1994).
- [6] R. van Roij, B. Mulder, and M. Dijkstra, *Physica A* **261**, 374 (1998); M. Dijkstra and R. van Roij, *Phys. Rev. E* **56**, 5594 (1997).
- [7] R. P. Sear, *Europhys. Lett.* **44**, 531 (1998); P. Bartlett, *J. Chem. Phys.* **109**, 10 970 (1998); P. B. Warren, e-print cond-mat/9807117.
- [8] M. Dijkstra, R. van Roij, and R. Evans, *Phys. Rev. Lett.* **81**, 2268 (1998).
- [9] M. Dijkstra, R. van Roij, and R. Evans, *Phys. Rev. Lett.* **82**, 117 (1999).
- [10] J. K. Percus, *The Many-Body Problem* (Interscience, New York, 1963).
- [11] W. G. Hoover and F. H. Ree, *J. Chem. Phys.* **49**, 3609 (1968).
- [12] L. V. Woodcock, *Nature (London)* **385**, 141 (1997); P. G. Bolhuis, D. Frenkel, S.-C. Mau, and D. A. Huse, *ibid.* **388**, 235 (1997).
- [13] J. L. Barrat, M. Baus, and J. P. Hansen, *Phys. Rev. Lett.* **56**, 1063 (1986); *J. Phys. C* **20**, 1413 (1987).
- [14] W. G. T. Kranendonk and D. Frenkel, *Mol. Phys.* **72**, 679 (1991).
- [15] D. A. Kofke, *Mol. Simul.* **7**, 285 (1991).
- [16] X. C. Zeng and D. W. Oxtoby, *J. Chem. Phys.* **93**, 4357 (1990).
- [17] A. R. Denton and N. W. Ashcroft, *Phys. Rev. A* **42**, 7312 (1990).
- [18] J. Han and J. Herzfeld, *Mol. Phys.* **82**, 617 (1994).
- [19] X. Cottin and P. A. Monson, *J. Chem. Phys.* **107**, 6855 (1997).
- [20] P. Bartlett, R. H. Ottewill, and P. N. Pusey, *J. Chem. Phys.* **93**, 1299 (1990); *Phys. Rev. Lett.* **68**, 3801 (1992).
- [21] M. D. Eldridge, P. A. Madden, and D. Frenkel, *Nature (London)* **365**, 35 (1993); *Mol. Phys.* **79**, 105 (1993); **80**, 987 (1993); **84**, 395 (1995); E. Trizac, M. D. Eldridge, and P. A. Madden, *ibid.* **90**, 675 (1997).
- [22] H. Xu and M. Baus, *J. Phys.: Condens. Matter* **4**, 663 (1992).
- [23] G. A. Mansoori, N. F. Carnahan, K. E. Starling, and T. W. Leland, Jr., *J. Chem. Phys.* **54**, 1523 (1971).
- [24] E. B. Smith and K. R. Lea, *Trans. Faraday Soc.* **59**, 1535 (1963).
- [25] A. Rotenberg, *J. Chem. Phys.* **43**, 4377 (1965).
- [26] P. H. Fries and J. P. Hansen, *Mol. Phys.* **48**, 891 (1983).
- [27] B. J. Alder, *J. Chem. Phys.* **40**, 2724 (1964).
- [28] G. Jackson, J. S. Rowlinson, and F. van Swol, *J. Phys. Chem.* **91**, 4907 (1987).
- [29] T. Biben and J. P. Hansen, *Europhys. Lett.* **12**, 347 (1990).
- [30] S. Asakura and F. Oosawa, *J. Chem. Phys.* **22**, 1255 (1954).
- [31] A. Vrij, *Pure Appl. Chem.* **48**, 471 (1976).
- [32] H. N. W. Lekkerkerker and A. Stroobants, *Physica A* **195**, 387 (1993).
- [33] S. Amokrane and C. Regnaut, *Phys. Rev. E* **53**, 1990 (1996).
- [34] Y. Rosenfeld, *Phys. Rev. Lett.* **72**, 3831 (1994); *J. Phys. Chem.* **99**, 2857 (1995).
- [35] S. Sanyal, N. Easwar, S. Ramaswamy, and A. K. Sood, *Europhys. Lett.* **18**, 107 (1992).
- [36] J. S. van Duijneveldt, A. W. Heinen, and H. N. W. Lekkerkerker, *Europhys. Lett.* **21**, 369 (1993).
- [37] P. D. Kaplan, J. L. Rouke, A. G. Yodh, and D. J. Pine, *Phys. Rev. Lett.* **72**, 582 (1994).
- [38] A. D. Dinsmore, A. G. Yodh, and D. J. Pine, *Phys. Rev. E* **52**, 4045 (1995).
- [39] A. Imhof and J. K. G. Dhont, *Phys. Rev. Lett.* **75**, 1662 (1995); *Phys. Rev. E* **52**, 6344 (1995).
- [40] W. C. K. Poon and P. B. Warren, *Europhys. Lett.* **28**, 513 (1994).
- [41] A. D. Dinsmore, P. B. Warren, W. C. K. Poon, and A. G. Yodh, *Europhys. Lett.* **40**, 337 (1997).
- [42] H. Xu and C. Barentin, *J. Phys.: Condens. Matter* **7**, L13 (1995).
- [43] C. Caccamo and G. Pellicane, *Physica A* **235**, 149 (1997).
- [44] F. Saija and P. V. Giaquinta, *J. Phys.: Condens. Matter* **8**, 8137 (1996).
- [45] T. Coussaert and M. Baus, *Phys. Rev. Lett.* **79**, 1881 (1997).
- [46] T. Coussaert and M. Baus, *Phys. Rev. Lett.* **80**, 4832(E) (1998); *J. Chem. Phys.* **109**, 6012 (1998).
- [47] F. Saija, G. Fiumara, and P. V. Giaquinta, *Mol. Phys.* **87**, 991 (1996); **89**, 1181 (1996); **92**, 1089(E) (1997); R. J. Wheatley, F. Saija, and P. V. Giaquinta, *ibid.* **94**, 877 (1998).
- [48] E. Enciso, N. G. Almarza, D. S. Calzas, and M. A. Gonzalez, *Mol. Phys.* **92**, 173 (1997); E. Enciso, N. G. Almarza, M. A. Gonzalez, and F. J. Bermejo, *Phys. Rev. E* **57**, 4486 (1998); see also D. Henderson and K. Y. Chan, *Mol. Phys.* **94**, 253 (1998).
- [49] C. Vega, *J. Chem. Phys.* **108**, 3074 (1998).
- [50] P. Attard, *J. Chem. Phys.* **91**, 3083 (1989); P. Attard and G. N. Patey, *ibid.* **92**, 4970 (1990).
- [51] R. Dickman, P. Attard, and V. Simonian, *J. Chem. Phys.* **107**, 205 (1997).
- [52] Y. Mao, M. E. Cates, and H. N. W. Lekkerkerker, *Physica A* **222**, 10 (1995).
- [53] T. Biben, P. Bladon, and D. Frenkel, *J. Phys.: Condens. Matter* **8**, 10 799 (1996).
- [54] B. Götzmann, R. Evans, and S. Dietrich, *Phys. Rev. E* **57**, 6785 (1998).
- [55] P. D. Kaplan, L. P. Faucheux, and A. J. Libchaber, *Phys. Rev. Lett.* **73**, 2793 (1994).
- [56] X. Ye, T. Narayanan, P. Tong, J. S. Huang, M. Y. Lin, B. L. Carvalho, and L. J. Fetters, *Phys. Rev. E* **54**, 6500 (1996).
- [57] Y. N. Ohshima, H. Sakagami, K. Okumoto, A. Tokoyoda, T. Igarashi, K. B. Shintaku, S. Toride, H. Sekino, K. Kabuto, and I. Nishio, *Phys. Rev. Lett.* **78**, 3963 (1997).
- [58] A. D. Dinsmore, D. T. Wong, P. Nelson, and A. G. Yodh, *Phys. Rev. Lett.* **80**, 409 (1998).
- [59] D. Rudhardt, C. Bechinger, and P. Leiderer, *Phys. Rev. Lett.* **81**, 1330 (1998).
- [60] R. Verma, J. C. Crocker, T. C. Lubensky, and A. G. Yodh, *Phys. Rev. Lett.* **81**, 4004 (1998).
- [61] A. P. Gast, C. K. Hall, and W. B. Russel, *J. Colloid Interface Sci.* **96**, 251 (1983).

- [62] J. P. Hansen and I. R. McDonald, *Theory of Simple Liquids* (Academic, London, 1986).
- [63] N. G. van Kampen, *Physica* (Amsterdam) **27**, 783 (1961).
- [64] R. van Roij and J. P. Hansen, *Phys. Rev. Lett.* **79**, 3082 (1997).
- [65] R. van Roij, M. Dijkstra, and J. P. Hansen, *Phys. Rev. E* **59**, 2010 (1999).
- [66] J. R. Henderson, *Mol. Phys.* **50**, 741 (1983).
- [67] Note that the factor $(1+q)^3$ in Eq. (31) is missing in Ref. [8]; it must be included, for nonvanishing q in order to obtain the correct low (η_2^r) density expansion.
- [68] A. Buhot and W. Krauth, *Phys. Rev. Lett.* **80**, 3787 (1998).
- [69] E. K. Hobbie, *Phys. Rev. E* **55**, 6281 (1997); E. K. Hobbie and M. M. Holter, *J. Chem. Phys.* **108**, 2618 (1998).
- [70] J. P. Hansen and L. Verlet, *Phys. Rev.* **184**, 151 (1969).
- [71] M. H. J. Hagen and D. Frenkel, *J. Chem. Phys.* **101**, 4093 (1994).
- [72] P. Bolhuis and D. Frenkel, *Phys. Rev. Lett.* **72**, 2211 (1994); P. Bolhuis, M. Hagen, and D. Frenkel, *Phys. Rev. E* **50**, 4880 (1994).
- [73] N. F. Carnahan and K. E. Starling, *J. Chem. Phys.* **51**, 635 (1969).
- [74] R. Hall, *J. Chem. Phys.* **57**, 2252 (1972).
- [75] W. H. Press, B. P. Flannery, S. A. Teukolsky, and W. T. Vetterling, *Numerical Recipes in Fortran* (Cambridge University Press, New York, 1992).
- [76] P. R. ten Wolde and D. Frenkel, *Science* **277**, 1975 (1997).
- [77] C. F. Tejero *et al.*, *Phys. Rev. Lett.* **73**, 752 (1994).
- [78] Y. Heno and C. Regnaut, *J. Chem. Phys.* **95**, 9204 (1991).
- [79] G. Stell, *J. Stat. Phys.* **63**, 1203 (1991).
- [80] A selection of recent papers is E. Z. Hamad, *J. Chem. Phys.* **103**, 3733 (1995); **107**, 6877 (1997); M. K. Khoshkbarchi and J. H. Vera, *Fluid Phase Equilibria* **142**, 131 (1998); M. K. Khoshkbarchi and J. H. Vera, *ibid.* **149**, 379 (1998); S. B. Yuste, A. Santos, and M. López de Haro, *J. Chem. Phys.* **108**, 3683 (1998); D. Henderson and K. Y. Chan, *ibid.* **108**, 9946 (1998); C. Caccamo, G. Pellicane, and E. Enciso, *Phys. Rev. E* **56**, 6954 (1997); D. V. Matyushov and B. M. Ladanyi, *J. Chem. Phys.* **107**, 5815 (1997); T. Boublik, *Mol. Phys.* **91**, 161 (1997); D. H. L. Yau, K. Y. Chan, and D. Henderson, *ibid.* **88**, 1237 (1996); M. Barošová, A. Malijevský, S. Labik, and W. R. Smith, *ibid.* **87**, 423 (1996); D. Henderson, A. Malijevský, S. Labik, and K. Y. Chan, *ibid.* **87**, 273 (1996); D. H. L. Yau, K. Y. Chan, and D. Henderson, *ibid.* **91**, 1137 (1997); A. Malijevský, M. Barošová, and W. R. Smith, *ibid.* **91**, 65 (1997).
- [81] E. J. Meijer and D. Frenkel, *J. Chem. Phys.* **100**, 6873 (1994).
- [82] After the publication of Ref. [9] we became aware of an error in one of the simulation curves ($\eta_1=0.1$) in Fig. 2 in Ref. [9]. In Fig. 13 we show the correct curve for $q=0.1$, which does not show the “dramatic” increase of η_2 for $\eta_2^r > 0.15$ as reported in [9].
- [83] K. G. Soga, J. R. Melrose, and R. C. Ball, *J. Chem. Phys.* **108**, 6026 (1998).
- [84] E. K. Hobbie, *Phys. Rev. Lett.* **81**, 3996 (1998).
- [85] P. N. Pusey, A. D. Pirie, and W. C. K. Poon, *Physica A* **201**, 322 (1993).
- [86] W. C. K. Poon, A. D. Pirie, M. D. Haw, and P. N. Pusey, *Physica A* **235**, 110 (1997); R. M. L. Evans and W. C. K. Poon, *Phys. Rev. E* **56**, 5748 (1997).
- [87] H. N. W. Lekkerkerker, W. C. K. Poon, P. N. Pusey, A. Stroobants, and P. B. Warren, *Europhys. Lett.* **20**, 559 (1992).
- [88] M. Dijkstra, *Phys. Rev. E* **58**, 7523 (1998).
- [89] H. N. W. Lekkerkerker (private communication): indeed including, by hand, a similar surface term as in Eq. (43) in the free volume approach also gives a good account of the simulation data.
- [90] R. Evans, R. J. F. Leote de Carvalho, J. R. Henderson, and D. C. Hoyle, *J. Chem. Phys.* **100**, 591 (1994).